Durham E-Theses

Analysing the atolls: X-ray spectral transitions of accreting neutron stars

Gladstone, Jeanette Claire

How to cite:

Use policy

ANALYSING THE ATOLLS: X-RAY SPECTRAL TRANSITIONS OF ACCRETING NEUTRON STARS

Jeanette Claire Gladstone

A thesis submitted to the University of Durham

in accordance with the regulations for

admittance to the Degree of Master of Science.

September 2006

X-Ray Sub-Group

Extragalactic Astronomy and Cosmology

Department of Physics

University of Durham

Abstract

Here we investigate disc accreting neutron stars with low magnetic fields (atoll sources) by systematically analysing all the available X-ray spectra of these sources from the *Rossi X-ray Timing Explorer* database, provided by the *High Energy Astrophysics Science Archive Research Center*.

From these we show that all atoll sources show broadly similar spectral evolution as a function of mass accretion rate with hard spectra at low luminosities switching to soft spectra at high luminosities. This is similar to the well known hard/soft spectral dichotomy in black holes. However, we also show that there are subtle but significant differences in the hard/soft transitions for individual atoll sources. There are two different types of hard/soft transition, those where the spectrum softens at all energies, leading to a diagonal track on a colour-colour diagram, and those where only the higher energy spectrum softens, giving a vertical track. The luminosity at which the transition occurs is *correlated* with this spectral behaviour, with the vertical transition at $L/L_{\mathrm{Edd}} \sim 0.02$ while the diagonal one is at ~ 0.1. Superimposed on this is the well known hysteresis effect, but we show that classic, large scale hysteresis occurs only in the outbursting sources, indicating that its origin is in the dramatic rate of change of mass accretion rate during the disc instability.

We show that the long term mass accretion rate correlates with the transition behaviour, and speculate that this is due to the magnetic field being able to emerge from the neutron star surface for low average mass accretion rates. While this is not strong enough to collimate the flow except in the millisecond pulsars, its presence may affect the inner accretion flow through changing the jet properties.

Contents

Declaration

The work described in this thesis was undertaken between 2004 and 2006 while the author was a research student under the supervision of Dr Christine Done in the Department of Physics at the University of Durham. This work has not been submitted for any other degree at the University of Durham or any other University.

Portions of this work have appeared in the following papers:

- Gladstone, J. C., Done, C., Gierliński, M., 2006, Monthly Notices of the Royal Astronomical Society (submitted), **Analysing the Atolls: X-ray Spectral Transitions of Accreting Neutron Stars**

Acknowledgements

Chapter 1

Introduction

The light we see when we look at the world around us, or up into the night sky, is only a small fraction of the 'light' in our Universe. Visible light is just a narrow band of the electro-magnetic spectrum and for millennia the only part visible to astronomers. It was not until the second half of the last century that astronomers were able to view the Universe in a greater variety of wavelengths, with the development of new technology to open ourselves to new realms of 'sight'.

With the exception of radio waves, part of the infra-red band and the optical band, the Earth's atmosphere blocks out most other radiation. To gather more information about our Universe we need to look at it from above our atmosphere. The advent of the space race enabled the development of satellites which, when outfitted with instruments and cameras, opened a new window on our Universe. It is now possible to detect a whole range of new 'colours' in the sky, from radio and infra-red to X-rays and γ-rays, impacting greatly on our understanding of the Universe.

This thesis uses data gathered by one such satellite, the *Rossi X-ray Timing Explorer (RXTE)*, a satellite launched just over a decade ago to concentrate on X-ray emitting objects both within our Galaxy and beyond. We will focus here on the emission from compact objects residing within our Galaxy, particularly those locked in binary systems containing low mass companion stars. Collectively these are known as Low Mass X-ray Binaries (LMXB). These compact objects fall into two groups; neutron stars (NS) and galactic black holes (GBH).

Over the years there has been considerable research into these objects helping us not only to develop our understanding of these objects but also our theories of gravity. Primarily these objects have been found in our Galaxy, although advancements in X-ray

sensitivity means that they are starting to be observed in others.

Observations over the last forty years have revealed that all LMXB systems exhibit the same signs of mass transfer from the companion star to the compact object through a process called Roche lobe overflow. This has allowed us to develop an understanding of accretion and disc structure without considering the type of object at its core. We cannot ignore the central object altogether though, as there should be a difference due to the presence (or absence) of a surface. As technology has developed, this predicted GBH and NS difference has been observed in the X-ray spectra and variability of these objects (see for example the review by Narayan 2005). Since then the majority of studies have focused on the more exotic of the two classes, those containing black holes, with some systematic studies looking at all known LMXB containing GBH. The same cannot be said for the neutron star sources. There are many studies of individual objects, but little in the way of systematic overviews of these sources and how they compare with GBH. This is the aim of this thesis.

Chapter 2
Compact Objects

Looking up at night sky it is possible to see thousands of stars with the unaided eye. Initially they all appear very similar, just small points of light against the black canvas of the night sky, but as we look closer we find that there are a wide variety of objects in our Universe of various colours and sizes. They may be hot blue stars, burning rapidly through the fuel contained in their core, or old red giants, living out the final days of their life (in stellar evolutionary terms). We also find that most points of light in our sky are not individual sources, that many are in groups of 2, 3 or more stars. These stars are locked together in orbit around one another by gravity. In the most extreme cases we may be looking at a whole galaxy of stars, so distant that we see them as one faint patch of light.

Current theory suggests that stars are formed in molecular clouds, large regions of (comparably) high density in the interstellar medium. Areas within these clouds become gravitationally unstable, perhaps with the collapse triggered by shockwaves from a supernova, forming protostars that are usually surrounded by a protoplanetary disc. As the collapse continues, more and more material is drawn in, increasing the pressure at its core until a temperature is reached that causes nuclear fusion reactions to start.

Stars usually then spend about 90% of their lifetime on the main sequence, in a balance between the inward force of gravity and the outward pressure force of gas kept hot by fusing of hydrogen to produce helium in the core. Once the fuel is consumed the pressure decreases and the balance is lost. The time taken for this to occur is determined by the stars initial mass. A larger star has a greater reservoir of fuel, but its greater gravity means it needs a higher temperature to balance this. Due to the exquisite sensitivity of the nuclear reaction rate to temperature, they actually run out of fuel faster than the low

3

mass stars.

Once the star has finally exhausted all of its fuel the collapse starts again, and the fate of the star varies according to mass. Stellar mass stars will collapse until they reach a state where electron degeneracy is enough to halt the compression due to gravity (according the Pauli exclusion principle). This type of compact object is known as a 'White Dwarf'. For stars larger than about $6M_\odot$ the degenerate core mass is greater than the Chandrasekhar limit of $\sim 1.4M_\odot$ triggering a supernova explosion. This blows off much of the mass surrounding the core as it crosses beyond the maximum mass which can be supported by electron degeneracy, instead it is neutron degeneracy that stops the collapse. Electrons combine with protons to form neutrons and neutrinos such that the only material left is highly compacted neutrons, hence the name of the compact object formed, a 'Neutron' star. If neutron degeneracy is still not enough to resist the cores collapse then it will continue until the matter is compressed into an infinitely small, infinitely dense singularity at the centre of a 'Black Hole'.

The blown-off outer layers of the dying stars include some of the heavier elements produced which may be recycled during new star formation. These heavy elements allow the formation of rocky planets as the cycle of star formation starts again.

2.1 White Dwarfs

White dwarfs (WDs) are the burned out core of a dead star, like the dying embers of a fire, slowly cooling as it fades away to become a black dwarf. WDs are approximately the size of the Earth with an average mass of $0.5 - 0.6M_\odot$. This causes it to be about 300,000 times more dense that the Sun, in fact a golf ball size piece of WD would weigh about a ton on the Earth. Most WDs are extremely hot, up to 20,000 degrees, hence the white light they emit. Due to their temperature and small surface area it can take a long time for their un-replenished energy to radiate away. This process is thought to take $\sim$25 billion years meaning that the Universe has not lasted long enough for this to occur. This
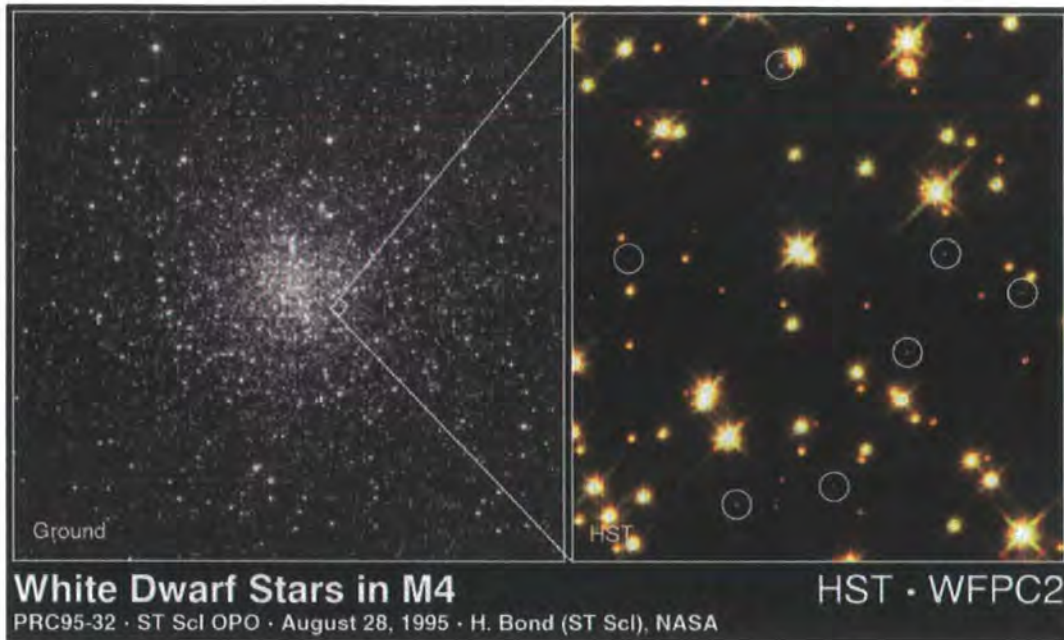
Figure 2.1: Images showing the discovery of eight white dwarfs in the M4 globular cluster by Harvey Richer and his team using the HST Wide Field and Planetary camera.

means that these objects can be used as 'cosmic clocks', giving an estimate to the age of the Universe independently of other techniques.

The first WD discovered was found (mainly) because its companion star, Sirius, is one of the brightest stars in our sky. In 1844 the astronomer Fredrick Bessel noticed a slight back and forth motion of the star but it was not until 1863 that the object causing the wobble was discovered by Alvin Grahem who labelled it a *dark companion* that appeared ten thousand times fainter than Sirius[1].

This faintness causes problems in finding more of these objects, for instance until just over a decade ago ground based and space based optical telescopes were only able to reveal a handful of WDs. That was until a study was carried out in August 1995 by an observing team led by Harvey Richer at the University of British Columbia, Vancouver, Canada.

---

[1]http://en.wikipedia.org/wiki/white_dwarf

They used Hubble data from the Wide Field and Planetary camera to make observations of the M4 globular cluster, located 7,000 light years away (the nearest globular cluster to the Earth). After only a few hours of observation time they were able to detect more than 75 WDs in just a small area of this old cluster. One such observation is shown in figure 2.1. The left hand image shows a view of the globular cluster containing more than 100,000 stars. The right hand image contains a Hubble colour image of a small part of the cluster revealing 8 of these objects (each circled) (see Hubble press release 1995 [2]).

2.2 Neutron Stars

Neutron stars (NS) are formed when massive stars die leaving a remnant collapsed core of $\sim 1.4 M_\odot$. This mass is packed into a core that is only about 10 kilometres across. This gives a density of $\sim 10^{14}$g/cc, about the density of an atomic nucleus, which means that if you had only a tea spoon of this on the Earth it would weigh about 5 tons. The dramatic collapse that compacts the core to form the neutron star tends to produce rapid rotations and very strong magnetic fields (up to 1000 rev s^{-1} and 10^{14} Gauss). The compactness of the core, along with the energy contained within it means that it has a temperature of about 100 million degrees. The small surface area gives rise to even more problems than for observing white dwarfs, they are incredibly dim in the optical band.

It was with the discovery of neutrons by Sir James Chadwick in 1932 that suggestions were made that a compact object made of these particles could exist, a so called neutron star which could be the result of a supernova. This idea was put forward by Walter Baade and Fritz Zwicky, although for many decades little time was given to the observation of these hypothetical objects as it was thought that they would be too small and too faint to make viable observations. This all changed dramatically in 1967 due to the studies of a graduate student called Jocelyn Bell and her supervisor Anthony Hewish. They were working on radio observations of quasars using a scintillation array constructed at the

---

[2]http://hubblesite.org/newscenter/newsdesk/archive/releases/1995/32/text

University of Cambridge. When examining observation charts produced by the array, Bell found a mark that appeared like clockwork once every $1^1/3$ seconds. Due to the regularity of the signal it was initially thought to be artificial but further analysis revealed that it was in fact extraterrestrial in origin. This was the discovery of the radio pulsar CP 1919 that earned Hewish the Nobel Prize in 1974. It was realised quite quickly through further research that pulsars were rotating neutron stars. Charged particles spiral down field lines to the magnetic poles of the NS. The beamed raditation then emitted rotates with the NS if the magnetic and rotational poles are miss-aligned. This creates a lighthouse effect when the beam sweeps across the field of view of an observer here on the Earth. This discovery renewed interest in these objects and led the discovery of many more. There are now more than 1000 known radio pulsars and this is just one variety of this type of compact object.

2.3 Black Holes

The compact object holding the highest position on the mass scale is a *Black Hole* (BH). These objects were theoretically predicted long before they were ever observed. It was a paper sent to the Royal Society by the English Geologist, John Mitchel that first suggested:

"If the semi-diameter of a sphere of the same density as the Sun were to exceed that of the Sun in the proportion of 500 to 1, a body falling from an infinite height towards it would have acquired at its surface greater velocity than that of light and consequently supposing light to be attracted by the same force in proportion to its vis inertiae(inertial mass), with other bodies, all light emitted from such a body would be made to return towards it by its own proper gravity."[3]

Although Mitchel found it unlikely he proposed, based on the Newtonian theory of gravity, that an object 500 times the radius of the Sun, with the same density as the Sun, would have an escape velocity that was equal to the speed of light. Therefore no light

---

[3]http://en.wikipedia.org/wiki/black_hole

could escape from it rendering the star un-observable to us.

Whilst being considered briefly by other scientists, it was not until 1915, when Albert Einstein developed his theories of gravity and general relativity that the concept of BHs was developed further. Around this time Karl Schwarzschild, using Einstein's theories, gave a solution for the gravitational field of a point mass showing that the objects now known as black holes could *theoretically* exist. The equation predicted a true singularity, a point mass with infinate curvature of space time. However, this is sheilded from the observer by an event horizon, the point at which the escape velocity is equal to the speed of light. This is at the Schwarzschild radius, $R_S = 2GM/c^2 \simeq 3 \times 10^3 \ M/M_\odot$. Slightly further out, at $3R_S$, is the last stable orbit, the smallest distance from the sigularity at which material can orbit the compact object. Schwarzschild like Mitchel, also thought that BHs where unlikely to be found as a physical reality.

In fact these hypothetical objects were still not given much thought until 1967 when both theoretical and experimental physics had progressed to such a stage that Roger Penrose and Steven Hawking were able to show that BHs were not only predicted by Einstein's theory of general relativity but that they would exist wherever sufficient mass was packed into a given region of space. Interest in these objects was renewed and shortly after this these objects were given the name (black holes) which they are known by today by the physicist John Wheeler.

Due to the inability to *see* inside the event horizon it means that, as Wheeler said, *"black holes have no hair"*. They can be modelled quite simplistically depending only of three parameters; mass, angular momentum or spin, and charge having no other features to distinguish them.

Considering the first of these *mass*, it should be noted that so far reference has only been made to stellar mass black holes, smaller BHs could be formed (in theory) if matter were subjected to sufficient pressure. It is thought that such conditions may have occurred during the early Universe when the temperature and pressure of the Universe was greater.
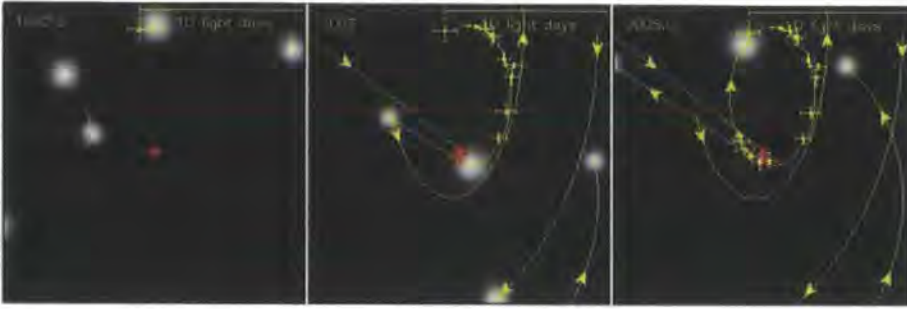
Figure 2.2: Three images taken from a simulation on the Max Plank Institutes Galactic Centre Research pages. They illustrate the affect of a supermassive block hole has on the region of space surrounding it. The stars motions can be used as an indirect method of observing this class of object.

In this situation density fluctuations may have caused primordial BHs to form, although they are yet to be observed.

Super massive black holes with mass 10^5 to $10^{10} M_\odot$, for example, are thought to be at the centre of most galaxies, including our own. The most compelling observational evidence for the existance of these sources is our own Galactic centre, by mapping the paths of stars close to the Galactic centre (as seen in figure 2.2 [4]), this shows that the stars paths are altered due to this gravitational attraction. This pattern could only occur if there is an object of super massive proportions, that is not optically visible to us, at the centre of the region of space considered.

All compact objects are difficult to see, and therefore to investigate. One way of learning more about them is by observing each type in binary systems. In this way it is possible to develop our understanding of these objects the their environments using the high energy radiation (X-rays) that are released from material being accreted onto the BH/NS or WD.

---

[4]http://www.mpe.mpg.de/ir/GC/index.php

Chapter 3

Matter Transfer Processes Theory for X-ray Binary Systems

Compact objects can be difficult to observe directly, the easiest way by far is if the black hole (BH), neutron star (NS) or white dwarf (WD) (as discussed in chapter 2) is contained within a binary system. This is because we can see the effects of the compact object on the companion clearly. Matter can be transferred to the compact object from the companion star and the large amount of gravitational energy released can be radiated in X-rays, giving them the name *X-ray binary* systems. The mechanisms that cause this energy release are explored in this chapter.

3.1 Matter Transfer - Roche Lobes

Material can be transferred from the companion to the compact object in two major ways, depending on the mass and separation of the binary system.

It was a French astronomer named Édouard Roche who developed the concept of the Roche lobe, a region of space around a star in a binary system within which orbiting material is gravitationally bound to that star. The shape of this is built up by plotting surfaces of equal potential (including terms for the centrifugal force as well as gravity). Close to each star (or object) these boundaries can be approximated to concentric spheres, moving further from each object the shape of the surface is distorted due to its companion until you reach a point where these surfaces intersect. This gives an approximate tear-
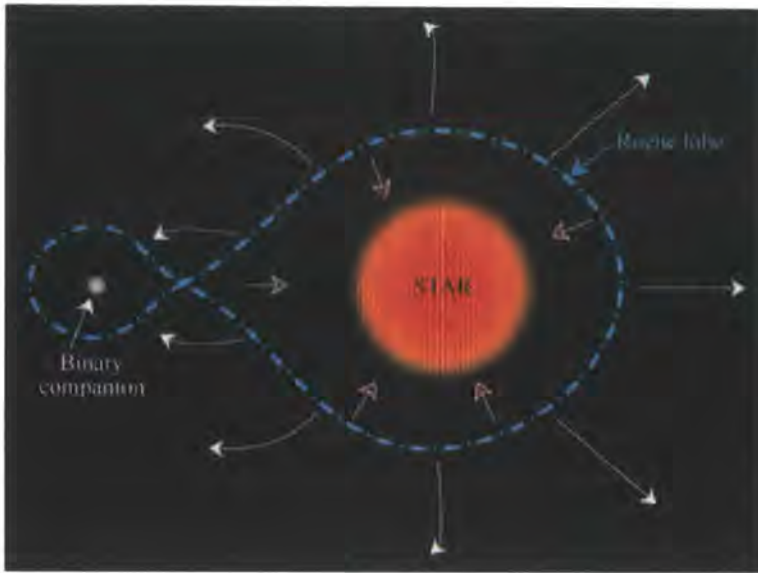
Figure 3.1:   Diagram to show mass transfer via stellar winds accreting
onto a compact object, known as wind fed matter systems (image from
http://cosmos.swin.edu.au/lookup.html?e=roche-lobe).

drop shaped region around each object, joining at the Lagrange point, the position where
the gravity of both objects effectively cancel out. This surface is labelled as the Roche
Lobe in figures 3.1 and 3.2.

Figure 3.1 shows a high mass star that has not filled its Roche lobe. In this case
matter cannot be transferred to the companion directly as it is gravitationally bound
to the star. However such high mass stars have strong winds from their surface, some
fraction of which can be captured by the compact object. This low angular momentum
wind may then feed the accretion process.

If the companion star is bound more tightly to the compact object it is possible that
the star will fill its Roche lobe (as shown in figure 3.2). In this case material at the
Lagrange point will feel an equal pull from both the star and the BH/NS or WD. This
allows material to flow across and drip feed the accretion process whilst slowly ripping
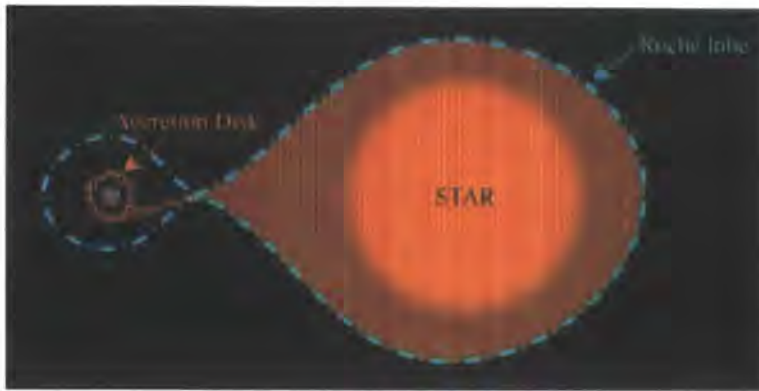
Figure 3.2: Roche lobe overflow, which can feed the accretion process in X-ray binary systems (image from http://cosmos.swin.edu.au/lookup.html?e=roche-lobe).

the star apart, by a process called Roche lobe overflow. Material crossing the boundary has a lot of angular momentum, so needs to lose this in order to accrete onto the compact object. If it is able to flow inwards then the gravitational energy released can power X-ray radiation. This can carry information about the accretion flow and the compact object at its core, including information on the size, mass, rotational rate and any residual magnetic fields of the object. The orbital periods of these objects can vary greatly from ~ 0.1 hours to 400 hours, found using the modulations due to eclipses, periodic X-ray absorption dips, etc. Trying to use this X-ray data to unravel this information requires an understanding of these systems and accretion theory.

3.2   X-Ray Binary Systems

X-ray binary systems contain a compact object and a companion star locked together by the force of gravity. If the compact object is a white dwarfs (WD) then the binary system is called a Cataclysmic Variable, or CV. However the much larger gravitational potential for black holes (BHs) and neutron stars (NS) means they produce much more high energy
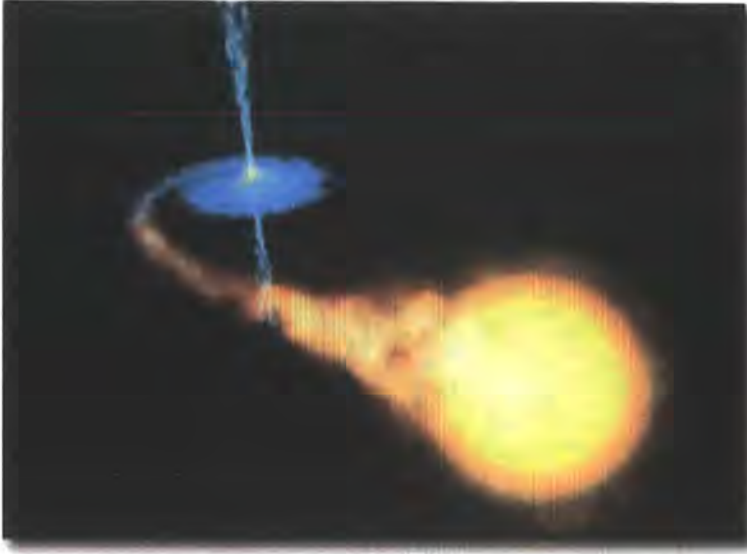
Figure 3.3: Artist impression of an accreting X-ray binary system (from en.wikipedia.org).

radiation. Therefore these sources are considered in greater detail below.

BHs and NS are held in either high mass or low mass X-ray binaries, shortened to HMXB and LMXB respectively. This name is not dependant on the mass of the compact object as black holes and neutron stars are part of both classes of system, it is related to the mass of the companion star.

3.2.1 High Mass X-ray Binaries (HMXB)

If the companion has a relatively high mass, usually a Be or type O star for example, the system is a high mass X-ray binary. In this case matter transfer can occur through either of the processes described above. In most cases part of the strong stellar wind from this star can be captured by the compact object, fuelling the accretion process. HMXB can also transfer matter transfer via Roche lobe overflow when the system is more compact.

Massive stars are very luminous and therefore easily detected, aiding the search for the optical counterparts of these sources. This also means that the massive star dominates

the emission of optical light but the compact object is the dominant source of X-rays, due to the energy released by accretion. One of the most famous HMXB was the first stellar-mass black hole discovered, Cygnus X-1, which is mainly powered by Roche lobe overflow.

3.2.2   Low Mass X-ray Binaries (LMXB)

When the companion star is of lower mass than that of our Sun, the system is a low mass X-ray binary. Such stars do not have strong stellar winds so accretion can only take place through Roche lobe overflow. An example of a LMXB source is Sco X-1, which was discovered during the first rocket flight to detect cosmic X-ray sources (for more information on these sources see chapter 4).

3.3   Accretion Theory

In this thesis we consider only low mass X-ray binary systems that are fed by Roche lobe overflow. Here we can use the standard models (and the physics behind them) that explain the passage of this mass from the point of overflow to the central compact object. In this case material leaves the companion and crosses the Lagrange point carrying a lot of angular momentum and must lose some of this in order to move in towards to central object. Using some basic assumptions it is possible to gain a great deal of insight into the processes involved, even using Newtonian gravity. For example, we can derive the maximum luminosity (from gravitational energy release and Virial theorem) that can be radiated as being:

$$L_{max} = \frac{GM\dot{m}}{2r_{in}}$$

Since M/r_{in} is similar for both BH and NS therefore they have similar gravitational fields so should have similar accretion flows. This equation seems to suggest that the

more material you push through the disc, the more luminous it will become. This could theoretically extend to infinity, giving an infinitely brights source. There is a point at which the outward pressure of the accreting luminosity is greater than the inward force of gravity, therefore a limit is imposed by nature. This cap is known as the Eddington limit. This can be found by:

$$L_{Edd} = \frac{4\pi G M m_p c}{\sigma_T} \simeq 1.3 \times 10^{38} \left(\frac{M}{M_\odot} \right) ergs\_s^{-1}$$

3.3.1 Optically Thick Accretion

The standard model of disc accretion was developed by Shakura & Sunyaev (1973). The major advancement to come from their work was that the optically thick accretion discs could be modelled independently of the viscous processes transporting angular momentum out of the disc. With the use of Newtonian gravity, change in gravitational potential and Virial theorem (as before) it is possible to derive how the temperature, T, depends on a given radius, R, finding that:

$$T \propto R^{-\frac{3}{4}}$$

From this we can see that the blackbody emission radiates through a range of temperatures throughout the disc. Summing these over all radii gives the complete disc spectrum, sometimes described as a multi-coloured blackbody. The maximum disc temperature is produced at the smallest radius, i.e. the last stable orbit for a BH or the surface for a NS. This maximum temperature is of the order $T_{max} \simeq (L/L_{Edd})^{\frac{1}{4}} (M/M_\odot)^{-\frac{1}{4}}$ keV so both galactic black hole and NS discs should emit at X-ray energies.

Variations in the mass accretion rate can change the amount of energy we see emitted from these sources, but the most dramatic changes can occur due to hydrogen instability. This can occur when the accretion disc surrounding the compact object is quite large, meaning that material towards the outer edge of the disc is cool. At low mass accretion
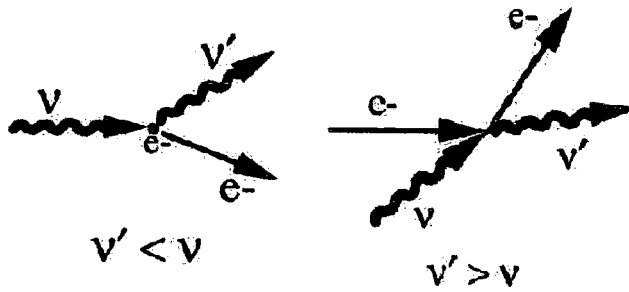
Figure 3.4: This image shows the processes and particles involved in Compton(a) and Inverse Compton(b) scattering (taken from http://venables.asu.edu/quant/proj/compton.html).

rates the hydrogen in the cool disc can therefore be mostly neutral. Fluctuations in the disc can increase the temperature in a region to a point at which hydrogen ionizes. This causes a dramatic instability to occur because the energy in that region can no longer escape, heating up the disc further, which causes more hydrogen to ionise so that more energy cannot escape heating up more of the disc, and so on and so forth. This runaway effect only stops when the disc becomes mostly ionized. Detailed calculations show that if the instability occurs anywhere in the disc, it will continue until it occurs everywhere in the disc. The whole disc becomes unstable causing an outburst of energy to occur.

3.3.2 Optically Thin Accretion

This assumes the flow is optically thick, so the energy can thermalise. This is not the case for low mass accretion rates. With lower accretion rates the flow becomes optically thin and the emission is no longer blackbody in nature. This means other forms of radiative emission must be considered, the most significant of which (for this thesis) is Compton scattering.

Compton scattering, or the Compton effect explains how energy is exchanged between

photons and electrons. This effect was observed in 1923 by Arthur Compton, which got him the Nobel Prize for Physics in 1927 because it demonstrated that light could not be explained purely as a wave. It is the collision of this particle of light (or photon) with an electron that results in the electron gaining energy as it recoils, so the photon loses energy. We can see this process in 3.4(a) showing the electron, in its rest frame, impacted by a high energy photon. Here energy is passed to the electron sending it off in one direction as the photon moves off in another.

However, if the electrons are relativistic, with more energy than the photons, the collisions result in the photon gaining energy, or being 'up-scattered' by the electron (inverse Compton scattering). Figure 3.4(b) shows this interaction between a photon and a high energy electron. The more collisions that occur, the more energy is given to the photons, increasing the hard component of the spectrum. There is a limit to this 'up-scattering' though, eventually the electrons and photons reach a stage of energy equilibrium so that when collisions occur the particle with the highest energy, whether photon or electron will give up some of that energy to the other particle.

Chapter 4

Observations of Accretion Flows in LMXB Systems

Since the initial (X-ray) observational discovery of both galactic black holes (GBHs) and neutron star (NS) sources there have been many observations made of these objects, with a wide variety of research taking place trying to develop and test our understanding of them. Much of the focus of the work has been on the more exotic of the two, black holes. Here we will focus on neutron stars so we review these sources below.

There are two main sub-categories of NS LMXB systems; atoll sources and Z sources, so named because of the shape they formed when they were first plotted on a colour-colour diagram (CCD) (see figures 4.1 and 4.2). The colours used to plot these are known as 'hard' colour and 'soft' colour, these are actually hardness ratios taken from the energy spectrum of these sources. They are used to give a general overview of the shape of a spectrum and how it evolves with time. The colours are created by separating the energy range into 3 or 4 bands, the ratio of the two lower bands forms the soft colour, while the two higher bands are used to get the hard colour. There is no clear definition for the choice of energy ranges used to calculate these ratios or colours. It is dependant on the authors choice and/or the detectors in use.

The distinction between atolls and Z sources is visible on the CCD but it can be more clearly seen in their X-ray timing properties. Z sources are able to trace out their path on a CCD on a timescale of hours to days. They also tend to be softer than atolls with the spectral and timing properties unique to each branch on the CCD, known as the
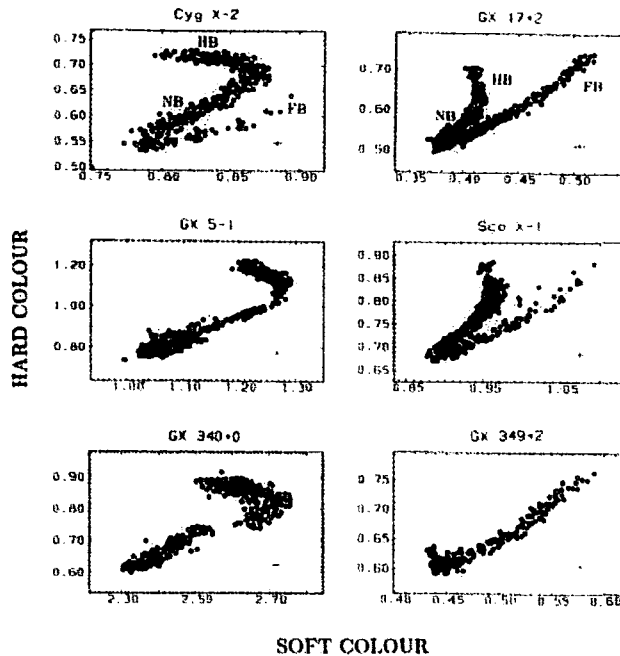
Figure 4.1: Colour-colour diagrams of the Z type neutron star LMXB taken from Hasinger and van der Klis 1989, labelling the three branches as follows: HB = horizontal branch, NB = normal branch and FB = flaring branch.

horizontal, normal and flaring branch, moving through each branch without jumping. As the mass accretion rate increases the spectrum seems to evolve such that it moves down through the Z shaped track whilst being persistently luminous, varying individually only within a relatively limited range ($1 < L/L_{Edd} < 3$) throughout their transitions. (See Hasinger & van der Klis 1989.)

Conversely the atoll sources are lower in luminosity with $L/L_{Edd} < 1$. The early plots of these sources on a CCD seemed to show a band of observations at a constant hard colour, varying in soft colour, labelled the banana branch, with 'islands' (known as the island state or island branch) appearing at higher hard colours as shown in figure 4.2. This gives a C (or atoll) structure on the CCD. Since then it has been discovered that this structure is only part of the full atoll track. With the greater quantity of data now
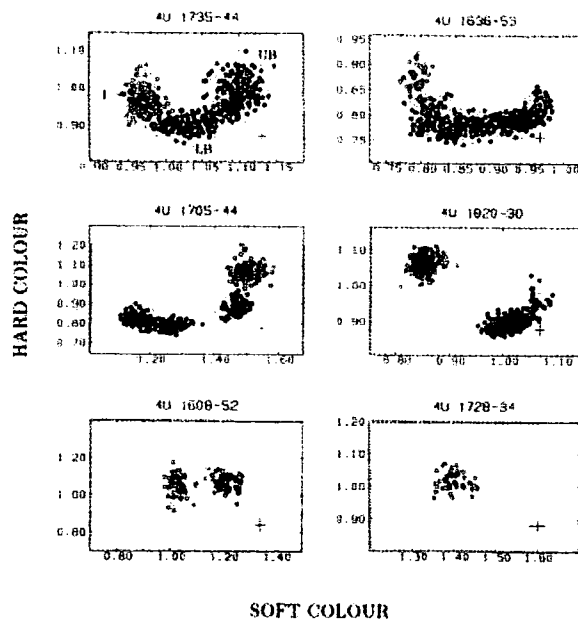
Figure 4.2: Colour-colour diagrams of the atoll type neutron star LMXB, again taken from Hasinger and van der Klis 1989. These plots show sources mainly in the banana branch whilst 4U 1820-30 also appears in the island state. The labels UB and LB refer to the upper banana and lower banana states.

available it is possible to track these sources to fainter levels. This reveals an additional branch which transforms the C shape to a Z shaped track on the colour-colour diagram. It should be noted that the Z structure presented in these new diagrams is due to the wider sampling of observations and is not implying they are to be reclassified as Z sources (see Muno, Remillard & Chakrabarty 2002 and Gierliński & Done 2002). Not all atoll sources trace out the full three branches. One reason for this is that some have stable discs, so their mass accretion rate does not sample the full range required to trace out the whole pattern. Alternatively, observation scheduling can mean that transitions are missed.

The long timescale evolution of these LMXB systems includes periods where the orbit

shrinks via magnetic torques. These can reduce the magnetic field strength from $\sim 10^{12}$G to $\sim 10^8$G, at which point it can be buried by the accretion flow (as seen in atoll sources). In some atoll systems, known as millisecond pulsars, the mass accretion rates are lower, consequently the magnetic field is not completely buried. This allows pulsations to occur as the accretion flow is channelled into the magnetic poles, giving a lighthouse effect as the neutron star rotates. So far these systems have only been observed in the island state.

As well as atoll and Z sources, there are also a number of sources which are difficult to classify. There are also some that display strong periodic intensity variations of there lightcurves due to dips and/or eclipses, these occur when the system is viewed at high inclinations, close to the plane of the accretion disc. In this case energy emitted from the compact object and part, or all of the inner disc is obscured by the companion star and/or the outer disc.

Many of the studies carried out so far have looked at individual sources from both GBHs and NS, although some have tried to gain an overview of the underlying physics involved by carrying out systematic survey of categories/sub-categories of sources. One such research project was published by Done & Gierliński in 2003, *Observing the effects of the event horizon in black holes* (referred to as DG03). In this paper they used the huge database now available from *RXTE* (for more details on this satellite see chapter 5) to build a picture of the X-ray spectral evolution as a function of overall mass accretion rate of a range of sources. DG03, however, chose to use intrinsic colours to get a broad idea of the range of spectral shapes given by these objects. Instead of defining the colours by the counts detected within a certain energy range, which depends on both the instrument response and the absorption column (N_H), they used intrinsic (absorption corrected) flux in the chosen energy bands so that they could directly compare different sources independent of their N_H.

They did this by modelling the source spectra. Both NS and GBH have similar accretion flows due to the similarity of their gravitational potentials although the presence of
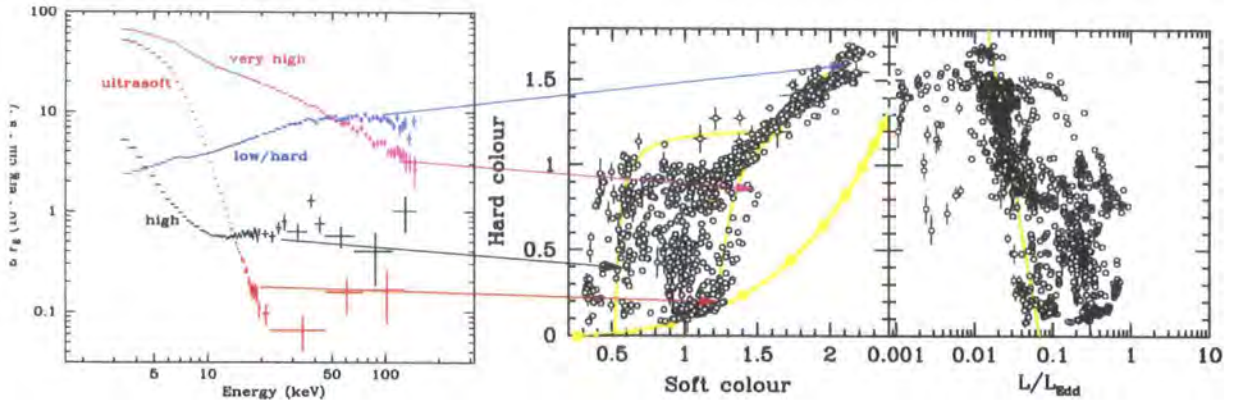
Figure 4.3: (a) illustrates the range of spectral states seen in GBH. (b) the intrinsic CCD and CLD for all GBH sources analysed in the DG03 study. The position is clearly shown of the hard and soft states on the CCD.

a surface implies an additional emission component is required to represent the boundary layer. They used data from GBH and disc accreting, low magnetic field NS (namely atolls and Z sources), finding that the atolls and GBH cover the same luminosity range in L/L_{Edd}. This varies from $\sim 10^{-3}$ to $\sim 0.5 - 1$, so their accretion flows should be directly comparable.

Their analysis illustrated the range of spectral shapes seen from GBH sources, four of which are given in figure 4.3(a). Despite the variety of spectral shapes a clear pattern emerges when they are plotted on a CCD (as seen in figure 4.3(b)). Figure 4.3(c) shows that while these spectral shapes are broadly correlated with the mass accretion rate with harder colours at lower luminosities, this is not a unique relation. Figure 4.4 shows the individual colour-colour and colour-luminosity diagram for six of the black holes included in 4.3. The individual plots show the switch from low/hard state to high/soft state can occur at different L/L_{Edd}. This is the well known hysteresis effect displayed by these sources.

The overall spectral evolution can be broadly explained if the X-ray emission from the
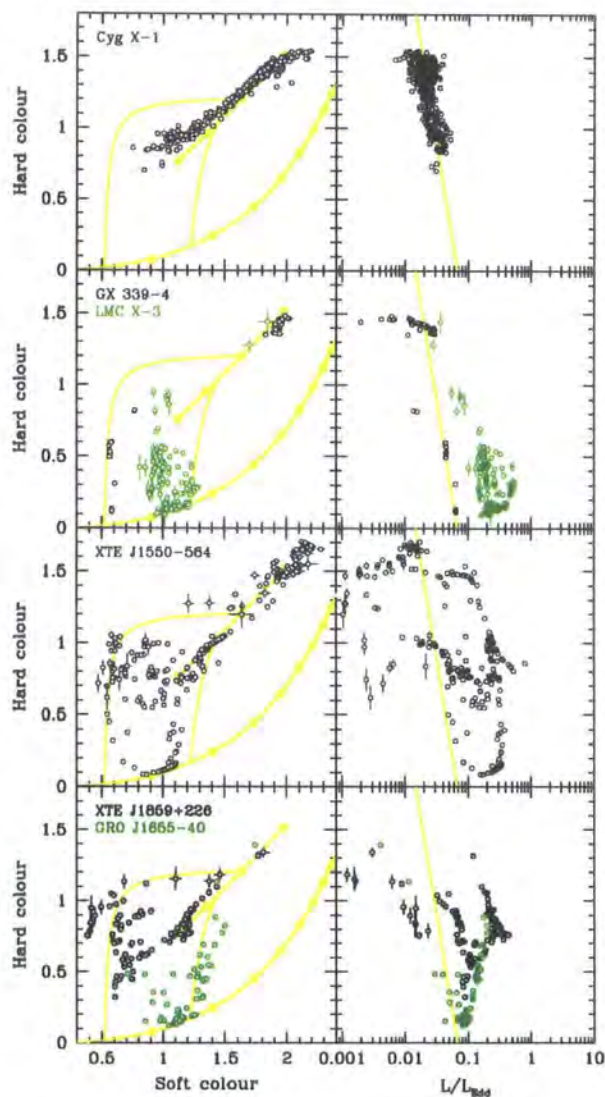
Figure 4.4: Colour-colour and colour-luminosity diagrams for six galactic black hole sources taken from Done & Gierliński (2003).
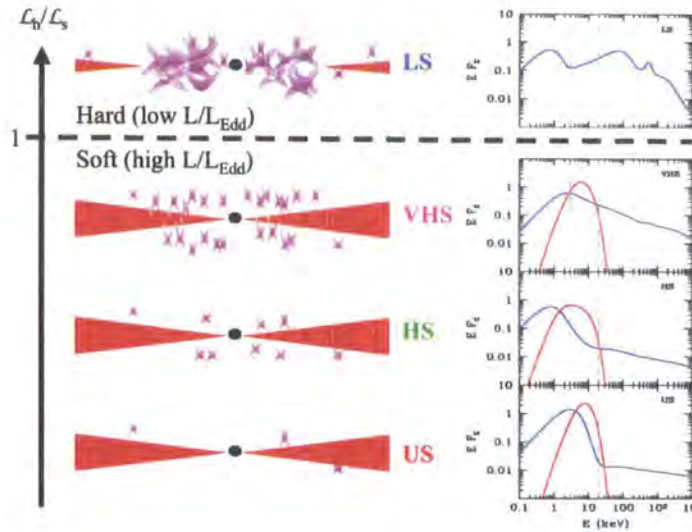
Figure 4.5: Models describing the states and spectra received from GBHs (plotted in blue) with the addition of a boundary layer componant (in red). This addition gives a good git to the spectra received from NS sources, from the conference proceeding by Done & Gierliński (astro-ph/04035462004).

system is dominated by an optically thin geometrically thick hot inner flow at low mass accretion rates. As the mass accretion rate increases the optically thick geometrically thin disc pushes inwards towards the compact object, creating a disc dominated soft spectrum. The left hand section of figure 4.5 shows a schematic picture picture for this changing geometry. This can be converted into qualitative models shown in the right hand side of this figure (blue spectra). This is more clearly seen in figure 4.6(a) which shows the colours created by these models. When compared with 4.6(b) we can see that the models span the same range of colours as the data.

DG03 also examined atoll sources in an attempt to observe the spectral impact of an event horizon/surface. These results confirmed the Z shaped track found previously on the CCD which is obviously different from the CCD of GBH (see figure 4.6(b)). This is consistant with expected boundary layer component in NS where the accretion flow
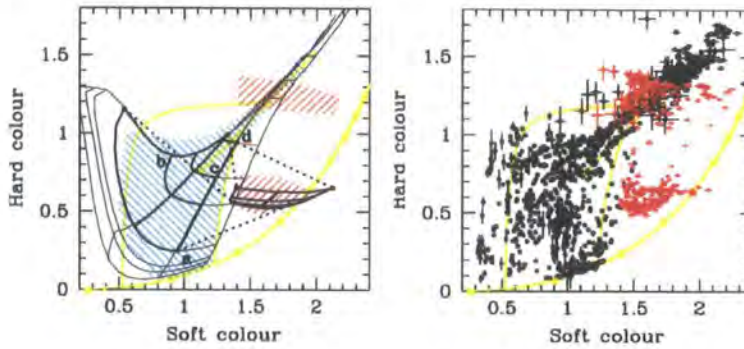
Figure 4.6: (a) The CCD shows the effect of an additional boundary layer component on the spectrum of a GBH. The soft state is transformed to a position that is co-spatial with the banana branch. (b) Plot from Done & Gierliński (astro-ph/04035462004) showing the work they achieved when looking at neutron stars and black holes in order to find the impact on X-ray spectra due to the presence/ absence of a surface. Here the GBH are open circles and the atoll sources are coloured red.

collides with the surface. Done & Gierliński showed that by incorporating a boundary layer component in their models for each GBH state (shown in red in the spectrum of figure 4.5) then the models predict the observed solours for NS (see figure 4.6(a)).

Figure 4.6(b), from DG03, displays their findings for all sources processed in this study. It showed that the GBH as a class were all consistent with the same spectral evolution as a function of mass accretion rate, as were the atolls, but this behaviour differed substantially between the two types of system even though they covered the same range in L/L_{Edd}. However, the sample of atolls used by Done & Gierliński was fairly small, with only 4 objects (1 of which was an accreting millisecond pulsar). This contrasts with their GBH selection, which included all available objects which were not heavily absorbed.

Here we present a much wider systematic study using all available atolls in $RXTE$ database which are not heavily absorbed, trying to gain an insight into the physics of these objects.

Chapter 5 | *Instrumentation*

5.1   The Rossi X-ray Timing Explorer

Launched on the 30th of December 1995 from the Kennedy Space Flight Centre using a Delta II rocket, the *Rossi X-ray Timing Explorer (RXTE)*, operated by NASAs Goddard Space Flight Centre (GSFC), was only initially designed for two years observational work in space, with a goal of 5 years. Ten years on and the *RXTE* satellite is still in a low-earth, 90 minute circular orbit, inclined at an angle of 23 degrees at an altitude of 580 km and it is still making major contributions to the scientific understanding of collapsed stars and compact objects.

The launch of this satellite gave the opportunity for the study of timing variability, tagging with an unprecedented timing resolution of microseconds. The three instruments mounted onboard (see figure 5.1) are the All Sky Monitor (ASM) and two pointed detectors, the High Energy X-ray Timing Experiment (HEXTE) and the Proportional Counter Array (PCA), with PCA and ASM data being co-ordinated by the Experiment Data System (EDS).

The EDS consists of 8 Event Analyzers (EAs), each containing an Intel 80286 processor and associated memory. The EAs can be programmed independently to process incoming events from the instruments, with 6 dedicated to the PCA data stream and 2 for ASM. The EAs are designed to work in parallel and bin individual events in order to fit the desired information into the telemetry constraints. The data is then transmitted via two NASA tracking and data relay satellites, through a ground station to the Science Operations Centre.

27
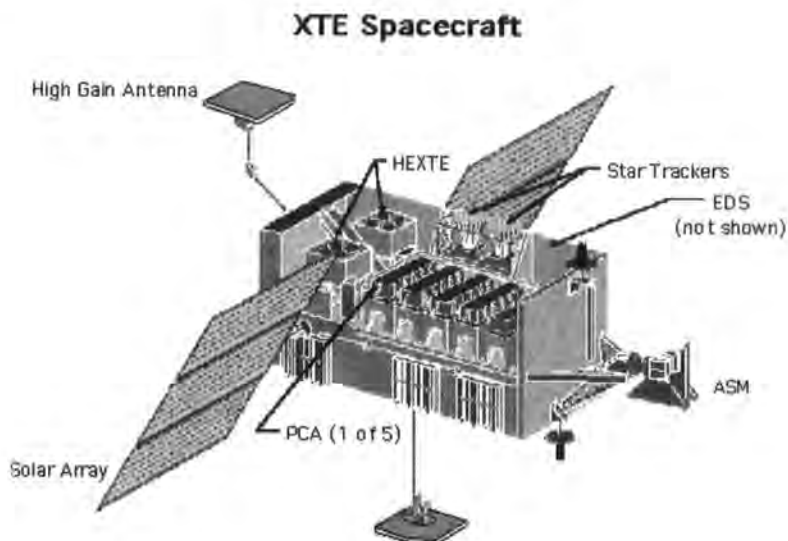
XTE Spacecraft

Figure 5.1: A schematic of the Rossi X-ray Timing Explorer *(RXTE)* spacecraft (from mamacass.ucsd.edu).

A summary of each of these detectors follows, but further details are available at the *RXTE* Technical Appendix (ftp://legacy.gsfc.nasa.gov/xte/nra/appendix f/).

5.1.1   All Sky Monitor (ASM)

The All Sky Monitor has its design and initial analysis team based at MIT. The detector consists of three wide angle cameras equipped with proportional counters giving a total collection area of 90cm ^{2} that can be rotated to view different regions of the sky by a motorized drive assembly. Each camera consists of a position sensitive Xenon proportional counter that can detect over a $1.5 - 12$ keV energy band with a sensitivity of ~ 30 mCrab.

Figure 5.2 shows ASMs ability to rotate to allow the instrument to monitor the long term behaviour of more than a thousand of the brightest X-ray sources and transients in
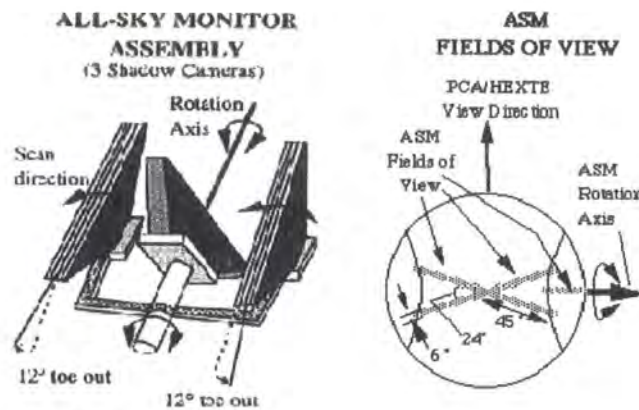
Figure 5.2: The All Sky Monitor (ASM) Assembly and fields of view (xte.mit.edu/xte_ASM.html).

view. By scanning in this way it observes about 80% of the sky every orbit. This means that it can also act as a sentinel, spotting targets of opportunity and manoeuvring the satellite quickly (within a few hours) to allow PCA and HEXTE to study the object.

5.1.2 Proportional Counter Array (PCA)

The Proportional Counter Array is composed of five proportional counter units (PCU 0-4) which combine to give a total effective area of 6250 cm^2. The experiment is used mainly in pointed observations and is sensitive to X-rays in the energy range of 2–60 keV.

As seen in figure 5.3(b), each PCU consists of hexagonal cells made of tin coated beryllium-copper sheets, behind which a multiwire proportional counter is installed, shielded by tantalum to reduce the cosmic X-ray background and the X-rays and γ-rays generated by cosmic ray impacts. This reduces the field of view to $\sim 1°$ and its design means that the detector can only observe targets and cannot measure the background simulta-
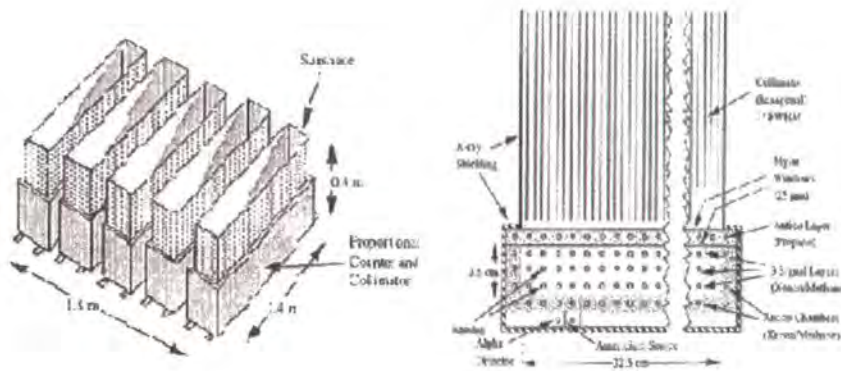
Figure 5.3: The Proportional Counter Array (PCA) assembly and cross-section of one counter (xte.mit.edu/xte_PCA.html).

neously. The background must be subtracted later by using accurate models produced by the instrumentation team. These include the cosmic X-ray background and the particle backgrounds induced by the combination of environment and the active spacecraft.

Once observed, each PCA event is processed onboard by the EDS to provide lightcurves with 0.125 seconds time resolution and no energy resolution (Standard-1) and a 129 channel energy spectrum every 16 seconds (Standard-2). Other modes are also available.

5.1.3 High Energy X-ray Timing Experiment (HEXTE)

The High Energy X-ray Timing Experiment was designed and built by the Center for Astrophysics and Space Sciences (CASS) at the University of California, San Diego. HEXTE consists of two clusters of detectors, each containing four phoswitch detectors collimated by a lead honeycomb. The clusters have the ability to rock or beam switch between mutually orthogonal directions in order to provide background measurements with an angular offset is ± 1.5 or ± 3.0 degree on either side of the on-source position. It has a field of view of 1 degree and the net open area of the eight detectors is $\sim 1600\ cm^2$, with each

counter detecting X-rays over the 15-250 keV energy range. The HEXTE instrument is also co-aligned with the PCA detector allowing for parallel observations over a much larger energy range.

Chapter 6

Observation

In this thesis we aim initially to gain an overview of the spectral evolution of low magnetic field, disc accreting neutron star sources (namely atolls) in order to develop our understanding of the physics behind these systems.

This work is also a continuation and development of that published by Done & Gierliński in 2003, entitled *Observing the effects of the event horizon in black holes* (hereafter in this chapter known as DG03), looking at a range of low mass X-ray binaries to try and understand the observational effects of an event horizon (or lack there of) on these systems. Therefore many of the sample constraints set out in that work are applied here, although in this case we look only at the neutron star sources.

6.1 Sample Selection

We searched the *RXTE* database for low magnetic field, disc accreting neutron star systems. We exclude Z sources (see A.1: Sco X-1, GX349+2, GX17+2, Cyg X-2, GX5-1, GX340+0, Cir X-1, LMC X-2) as we were interested in the range $10^{-3} < L/L_{Edd} < 1$ to compare with the galactic black holes from DG03.

We also exclude all objects with heavy absorption, defined as $N_H > 3 \times 10^{22}$ cm^{-2}, as above this the spectral decomposition becomes more uncertain. Given that most systems are in the Galactic plane, this removes many objects (see A.1: 4U 1624-49, GRO J1744-28, GRS 1747-312, SAX J1747.0-2853). The absorption criteria also excludes objects where there is substantial intrinsic absorption. This can be continuous, completely blocking our view of the continuum source so that the only scattered flux is seen (accretion disc corona sources), or the absorption can be episodic, giving discrete dips in the lightcurve

33

(dippers). We exclude all accretion disc corona sources (2S 0921-630, 4U 1624-49, 4U 1822-371, MS 1603+206), and dippers where the absorption events are so frequent that most observations are affected by them (EXO 0748-676), but we do include dippers where the absorption is limited to contaminating only a few observations (which we remove).

The application of the above selection criteria gave a total of 35 atoll sources and 6 millisecond pulsars. Table 6.1 give a brief summery of the properties of the selected sources. Alternate names for these sources, positions and references can be found in table 6.2. Those neutron star low mass X-ray binary sources that are not included are shown in these tables can be seen in A.1.

6.2 Data

The standard products 0.125 second time resolution light curves for all the available data for selected sources were downloaded and processed (using FTOOLS - lcstats) in order to find the rms variability of each observation. They were initially processed on a 0.125 second timing (with the maximum number of bins) to highlight any bursts occurring during each observation. A cut of 50% rms variability was taken as a marker for these, with any light curves showing values higher that this checked visually to confirm the bursts. The lightcurves were then reprocessed with lcstats on 16 second binning to filter out any observations contaminated by dips using a cut of rms > 20%. Again, all those selected by the cut were scanned visually to check for dips. These observational IDs were then removed, allowing the remaining standard products spectra (and associated background and response files) from the Proportional Counter Array, available from the High Energy Astrophysics Science Archive Research Centre (HEASARC) database to be gathered for each source, giving a total of about 3000 spectra to be downloaded.

Source Name	N_H (10^{22} cm^{-2})	Distance (kpc)	State or Transition	Dips	Period (hrs)	Spin (Hz)
4U 0614+091	0.28	3	T		1	
4U 0919–54	0.32	4.9	T		1	
4U 1254–690	0.291	13	B	Y	3.9	
4U 1543–624	0.27	7	B		0.3	
4U 1556–605	0.296	4	B		9.1	
4U 1608–52	1.5	3.6	T		288	619
4U 1626–67	0.069	8	I		0.68	
4U 1636–53	0.37	5.9	T		3.9	582
4U 1702–43	1.2	7.3	T			330
4U 1704–30	0.35	12	T	Y	4.2	567
4U 1705–44	1.47	7.4	T			
4U 1708–40	2.9	8	B			
4U 1711–35	1.5	8	T			
4U 1724–307	1	6.6	T	Y		
4U 1728–16	0.232	5	B			
4U 1728–34	2.5	4.75	T			363
4U 1730–33	1.6	8	B			
4U 1735–44	0.46	9.2	B		4.65	
4U 1744–26	1.76	8.5	B			
4U 1746–37	0.295	10.7	T	Y	5.16	
4U 1755–33	0.3	4	I	Y	4.4	
4U 1758–20	1.433	8.5	B			
4U 1812–12	1.6	4	I			
4U 1820–303	0.24	5.8	T		0.19	
4U 1837+04	0.51	8.4	B			
4U 1850–08	0.39	6.8	T		0.35	
4U 1908+005	0.96	2.5	T		19	549
4U 1915–05	0.2	9.3	T	Y		272
GS 1826–236	2.4	6	I		2.1	611
KS 1731–26	1	7	T			524
SLX 1732–304	1.2	15	B	Y		
SLX 1735–269	1.47	8.5	T			
XTE J1709–267	0.44	8.8	T			
XTE J1806–246	0.5	8	T			
XTE J2123–058	0.66	8	T			
IGR J00291+5934	2.8	4	I		2.46	599
XTE J0929–314	0.21	10	I		0.73	185
XTE J1751–305	1.01	8	I		0.7	435
XTE J1807–294	0.5	8	I		0.67	190
XTE J1808–369	0.122	3.15	I		2	401
XTE J1814–338	0.167	8	I		4.27	314

Table 6.1: A list of properties of atoll (above the dividing line) and millisecond pulsar (below the line) sources with observations available from the *RXTE* database. For *States* or *Transitions* I represents those sources that only appear in island state within the colour-colour diagram, B sources are only seen in the banana branch and T is displayed when a transition occurs between states.

Source Name	Alternate Name	RA	DEC	References
4U 0614+091		06 17 07.3	+09 08 13	1,2,4
4U 0919-54	2S 0918-549	09 20 26.52	-55 12 25.3	4,6,7
4U 1254-690	GR Mus	12 57 37.2	-69 17 21	1,3,8,9,10,11
4U 1543-624		15 47 54.29	-62 34 11.2	3,4,7,12,13,14
4U 1556-60		16 01 02.3	-60 44 18	1,3
4U 1608-52	GX 331-01	16 12 43.0	-52 25 23	1,3,15,16,17
4U 1626-67		16 32 16.8	-67 27 43	18,19,20
4U 1636-53		16 40 55.5	-53 45 05	1,15,21
4U 1702-43	Ara X-1	17 06 15.31	-43 02 08.7	1,3,5,8
4U 1704-30	MXB 1659-298	17 02 06.54	-29 56 44.1	22,23,24
4U 1705-44		17 08 54	-44 05.4	1,3,25
4U 1708-40		17 12 23.00	-40 50 36.0	26
4U 1711-34	2S 1711-339	17 14 19.20	-34 02 58.0	1,27
4U 1724-307		17 27 33.2	-30 48 07	1,8,28,29
4U 1728-16	GX 9+9	17 31 44.2	-16 57 42	1,2,3,30
4U 1728-34	GX 345-0	17 31 57.4	-33 50 05	1,15,31,32,33
4U 1730-33	Rapid Burster	17 33 24.10	-33 23 16.0	1,3,34
4U 1735-44		17 38 58.3	-44 27 00	1,2,3,5,35
4U 1744-26	GX3+1	17 47 56.0	-26 33 49	1,2,3,5
4U 1746-37		17 50 12.7	-37 03 08	1,3,8,36,37
4U 1755-33		17 58 40.0	-33 48 27	38,39
4U 1758-20	GX 9+1	18 01 32.3	-20 31 44	1,2,3,5
4U 1812-12		18 15 12.00	-12 05 00.0	1,39
4U 1820-303		18 23 40.45	-30 21 40.1	1,3,40
4U 1837+04	Ser X-1	18 39 57.5	+05 02 09	1,3,5
4U 1850-08		18 53 04.86	-08 42 20.4	3,41,42
4U 1908+005	Aql X-1	19 11 16.0	+00 35 06	1,3,15,17,43
4U 1915-05	2S 1912-05	19 18 47.78	-05 14 11.2	1,3,8,44,45,46,47
GS 1826-238		18 29 28.2	-23 47 49	1,48,49,50
KS 1731-260		17 34 13.45	-26 05 18.7	1,15,48,51,52
SLX 1732-304		17 35 46.88	-30 29 00.4	53
SLX 1735-269		17 38 16.00	-27 00 16.0	1,48,54,55
XTE J1709-267		17 09 30.20	-26 39 27.0	56
XTE J1806-246		18 06 50.20	-24 35 15.0	1,57,58
XTE J2123-058		21 23 14.54	-05 47 52.9	1,59

Source Name	Alternate Name	RA	DEC	References
IGR J00291+5934		00 29 03.06	+59 34 19.0	60,61,62
XTE J0929−314		09 29 18	-31 23.1	61,63,65
XTE J1751−305		17 51 16	-30 37.5	61,63,64,65
XTE J1807−294		18 06 59.8	-29 24 30	61,63
XTE J1808−369	SAX J1808.4−3658	18 08 27.54	-36 58 44.3	17,61,63,66
XTE J1814−338		18 13 39.03	-33 46 22.3	61,67,68

Table 6.2: This includes alternate (popular) names for selected sources, their ICRS 2000.0 coordinates (taken from SIMBAD) and the references used to acquire information on these sources. References: [1]Liu et al. 2001, [2]Schultz 1999, [3]Christian & Swank 1997, [4]Nelemans et al. 2003, [5]Fender & Hendry 2000, [6]Jonker et al. 2001, [7]Juett & Chakrabarty 2003, [8]Diaz Trigo et al. 2005, [9]Smale et al. 2002, [10]Courvoisier et al. 1986, [11]t Zand et al. 2003, [12]Shultz 2002, [13]Wang & Chakrabarty 2004, [14]Farinelli et al. 2003, [15]Piro & Bilsten 2005, [16]Gierliński & Done 2002, [17]Garcia et al. 2001, [18]Owens et al. 1997, [19]Chakrabarty 1997, [20]Angelini et al. 1995, [21]Wijnands 2001, [22]Oosterbroek et al. 2001, [23]Wijnands et al. 2001, [24]Oosterbroek et al. 2001, [25]Di Salvo et al. 2005, [26]Migliari et al. 2002, [27]Wilson et al. 2003, [28]Molkov et al. 2000, [29]Emelyanov et al. 2002, [30]Yao & Wang 2005, [31]Di Salvo et al. 2000, [32]Shaposhnikov et al. 2003, [33]Migliari et al. 2003, [34]Falanga et al. 2004, [35]Cornelisse et al. 2000, [36]Jonker et al. 1999, [37]Balucinska-Church et al. 2003, [38]Park et al. 2004, [39]Barret et al. 2003, [40]Shaposhnikov & Titarchuk 2004, [41]Sidoli et al. 2005, [42]Homer et al. 1996, [43]Chevalier et al. 1999, [44]Blosser et al. 2000, [45]Chevalier et al. 1999, [46]Maccarone & Coppi2002 [47]Galloway et al. 2001, [48]Barret et al. 1999, [49]Galloway at al. 2003, [50]Thompson et al. 2005, [51]Mignani et al. 2002, [52]Burderi et al. 2002, [53]Pavlinsky et al. 2000, [54]Molkov et al. 2005, [55]Wijnands & van der Klis 1999, [56]Jonker et al. 2004, [57]Wijnands & van de Klis 1999, [58]Revnivtsev et al. 1999, [59]Tomsik et al. 2004, [60]Galloway et al. 2005, [61]Poutanen 2005, [62]Jonker et al. 2005, [63]Campana et al. 2005, [64]Campana et al. 2003, [65]Gierliński & Poutanen 2005, [66]Wijnands 2003, [67]Krauss et al. 2005, [68]Strohmayer et al. 2003.

Chapter 7

Data Analysis and Results

Following the methods of Done & Gierliński (2003) (previously referred to as DG03), 1% systematic error was added to each energy band of the downloaded standard products *RXTE* PCA spectra using FTOOLS. The selected data files were then fit using a model of the disc emission and a Comptonised continuum, described by DISKBB (Mitsuda et al. 1984) and THCOMP (Zdziarski et al. 1996) in XSPEC, together with a smeared edge and Gaussian line to approximately mimic the reflected spectrum. The absorption column was fixed according to the values shown in Table 6.1. This model gave a good fit to all the spectra ($\chi^2_\nu < 1.5$).

The best-fitting model for each spectrum was integrated to form intrinsic soft and hard colours (i.e. absorption corrected and independent of the instrument response), defined as flux ratios in the bandpasses 4–6.4/3–4 and 9.7–16/6.4–9.7 keV, respectively. The unabsorbed model was also used to estimate the bolometric flux in the 0.01–1000 keV bandpass, and this converted into a luminosity using the distance estimate given in Table 6.1. As discussed by DG03, the colours are fairly robust to changes in the model spectra as long as the source is not heavily absorbed and the advantage of using intrinsic colours (as opposed to the more widely used instrument colours) is that many objects can be directly compared on the same plot. The bolometric fluxes are more uncertain though, as the model is extrapolated outside of the observed energy bandpass. Nonetheless, this model corresponds to expected physical components, and we fix a lower limit to the disc temperature of ≥ 0.4 keV and an upper limit to the Comptonising temperature of ≤ 100 keV so the continuum components cannot produce arbitrarily large luminosities in
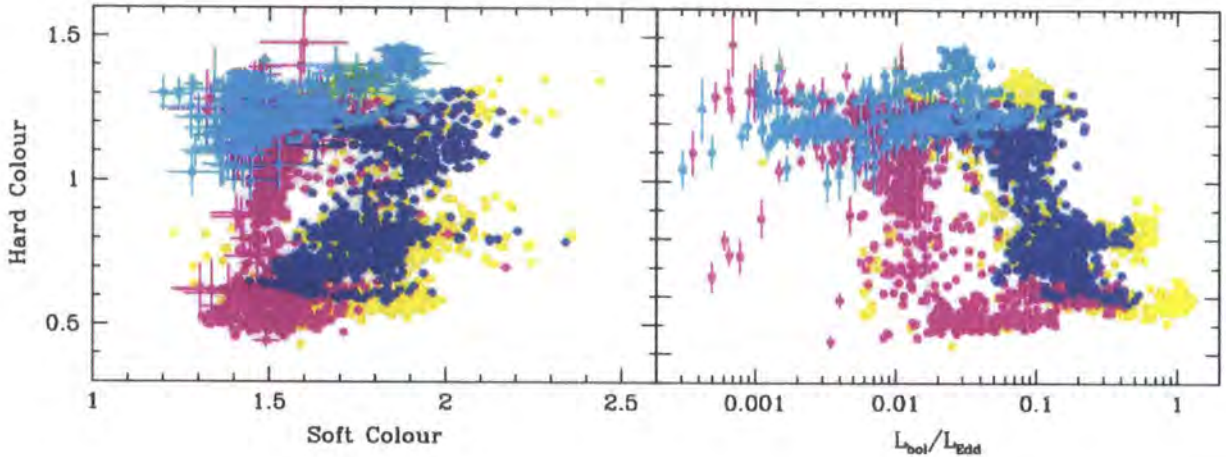
Figure 7.1: Combined colour-colour colour-luminosity plots for the *RXTE* PCA data of all atoll sources with $N_H < 3 \times 10^{22}$ cm^{-2}. It is clear that two distinct tracks have emerged, the magenta track occurring on the plots above shows a vertical transitions highlighting that only the higher energies appear to be softening, whilst a diagonal track is highlighted in blue, suggesting the spectrum is softening at all energies, with the millisecond pulsars in cyan overlaid on a yellow back drop of all data. It should be noted that an individual source will only follow one of these tracks.

the unobserved energy ranges (DG03).

Figure 7.1(a) shows that while the atolls displays the same overall behaviour as claimed by DG03, they also show subtle but significant differences. This is most evident in terms of the spectral evolution during the transition between the hard (island) and soft (banana) spectral states, which forms the middle branch of the total Z-shaped track on the colour-colour diagram (even though these are atolls, not Z sources). We have highlighted this by picking out in magenta those objects where the transition makes an almost vertical track on the colour-colour diagram (hereafter called verticals), while the blue symbols show those where the transition from island to banana starts much further to the right on the colour-colour diagram, but ends at approximately the same place, making a much

more diagonal middle branch (hereafter called diagonals). This difference in spectral evolution is also picked out in the colour-luminosity diagram as a different luminosity for the hard-soft transition. While the distances are generally rather uncertain, this correlation between the behaviour on the colour-colour and colour-luminosity diagrams give some confidence in the reality of the luminosity difference. We stress that this is not primarily due to hysteresis, the well known effect in both black holes and neutron stars where the luminosity at which the hard-soft transition occurs varies considerably in the same object. Here, the transition luminosity is varying between different objects.

Some of these differences could be connected to spin/inclination effects and the residual magnetic fields which may affect the environment surrounding the neutron star, and therefore the spectra seen. Transient behaviour and hysteresis may also be a cause of these effects as well as the short or long term mass accretion rate. Here we will attempt the test some of the main theories put forward and use these to speculate on the behaviour of these objects and the affect they have on their environment.

The majority of sources show well defined transition luminosities (to within a factor 2–3), irrespective of whether the transition is from hard to soft i.e. on the rising part of the light curve, or from soft to hard i.e. with a decreasing flux. However, there are two sources where the transitions have a much large scatter in their properties, namely 4U 1608–52 and 4U 1908+005. The colour-colour and colour-luminosity diagrams for these are plotted as the bottom two panels in figure 7.3, but it is not clear from the data that these sources should be classed as verticals or as a third type bridging between the two classes, so here we examine them in more detail.

These two systems are also the only two (apart from the millisecond pulsars) which show large scale outbursts. In order to investigate their scatter in transition behaviour we select simple outbursts from the light curve, where there is a clear fast rise followed by a monotonic decay. From these observations we build a new, simplified colour-luminosity diagram (figure 7.2). The cyan points show the island state seen on the rise. We then
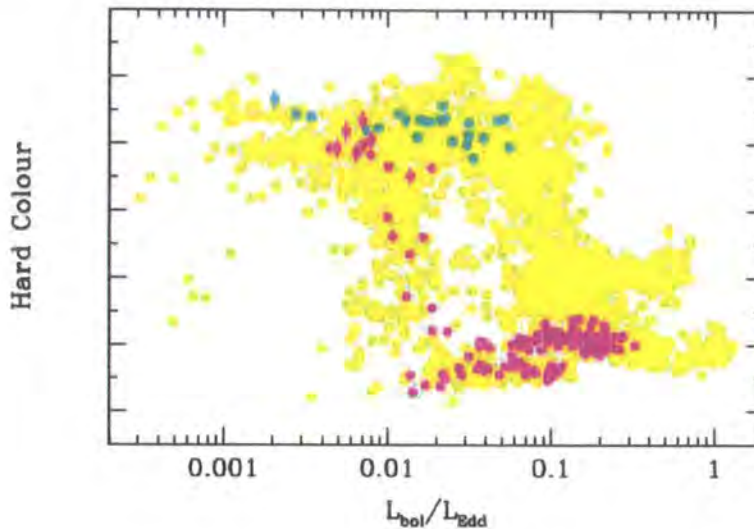
Figure 7.2: Colour luminosity diagram to highlight the track followed by 4U 1608-522 and 4U 1908+005 during hysteresis, plotted against that background of all observations. In cyan you can see the initial stages of the outburst (in cyan) match that of the msp, with the outburst decay shown in magenta, supporting the suggestion that if msp every made the transition they would display a vertical transition.

exclude all of the transition data on the rise/peak of each outburst, and plot the remaining banana branch and transition back to island state on the decay as the magenta points. Plainly the transition luminosity is much larger in the rise to outburst than during the decay. This effect of hysteresis is also seen in most galactic black holes. Plainly, the data during the fast rise look very similar to those from the millisecond pulsars, while the data taken during the slow decay confirm that these two sources are making a vertical transition.

None of the diagonals show marked hysteresis (> factor 2), though 4U 1705–44 and KS 1731–26 may show a small effect in that their top branch (island state) extends to higher luminosities than seen during the transition (figure 7.4). A similar small hysteresis effect may also be present in the vertical 4U 0919–54.

Figure 7.3: Combined colour-colour colour-luminosity plots for the *RXTE* PCA data of all atoll sources with $N_H < 3 \times 10^{22}$ cm^{-2} which display a vertical transition from hard to soft state in the colour-colour diagram, plotted against a backdrop of all data.

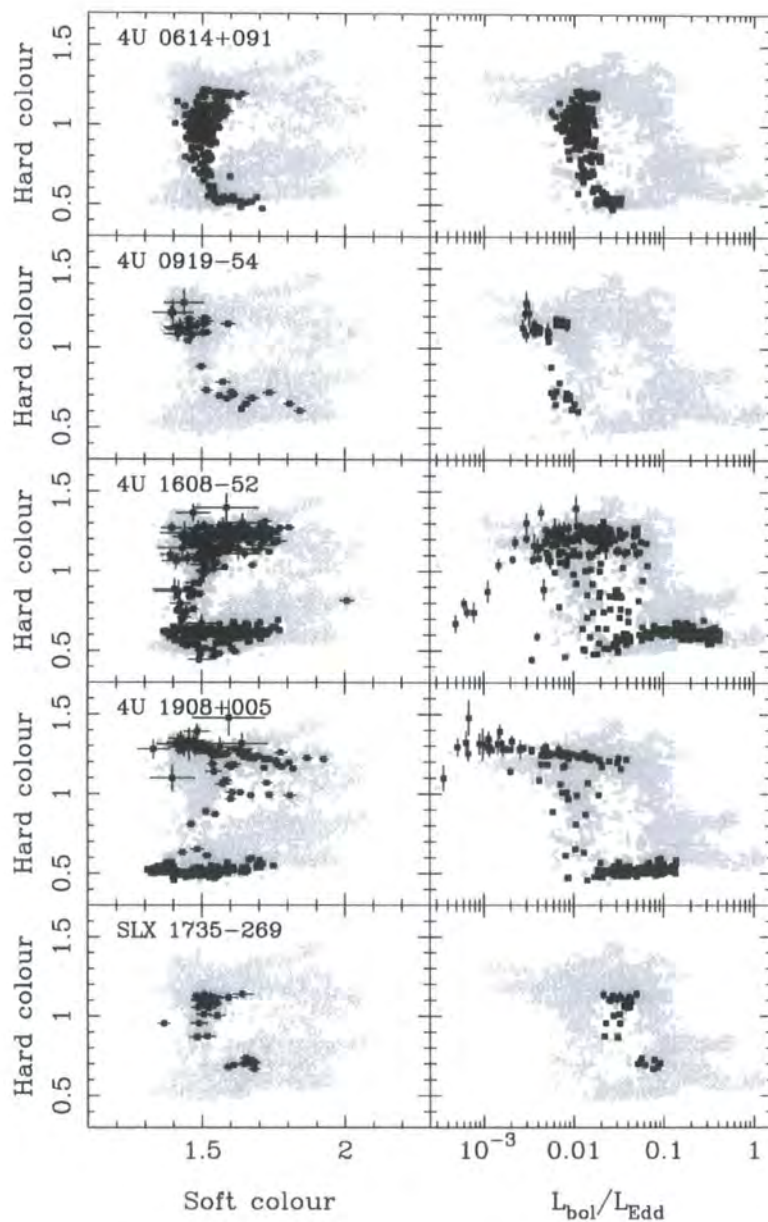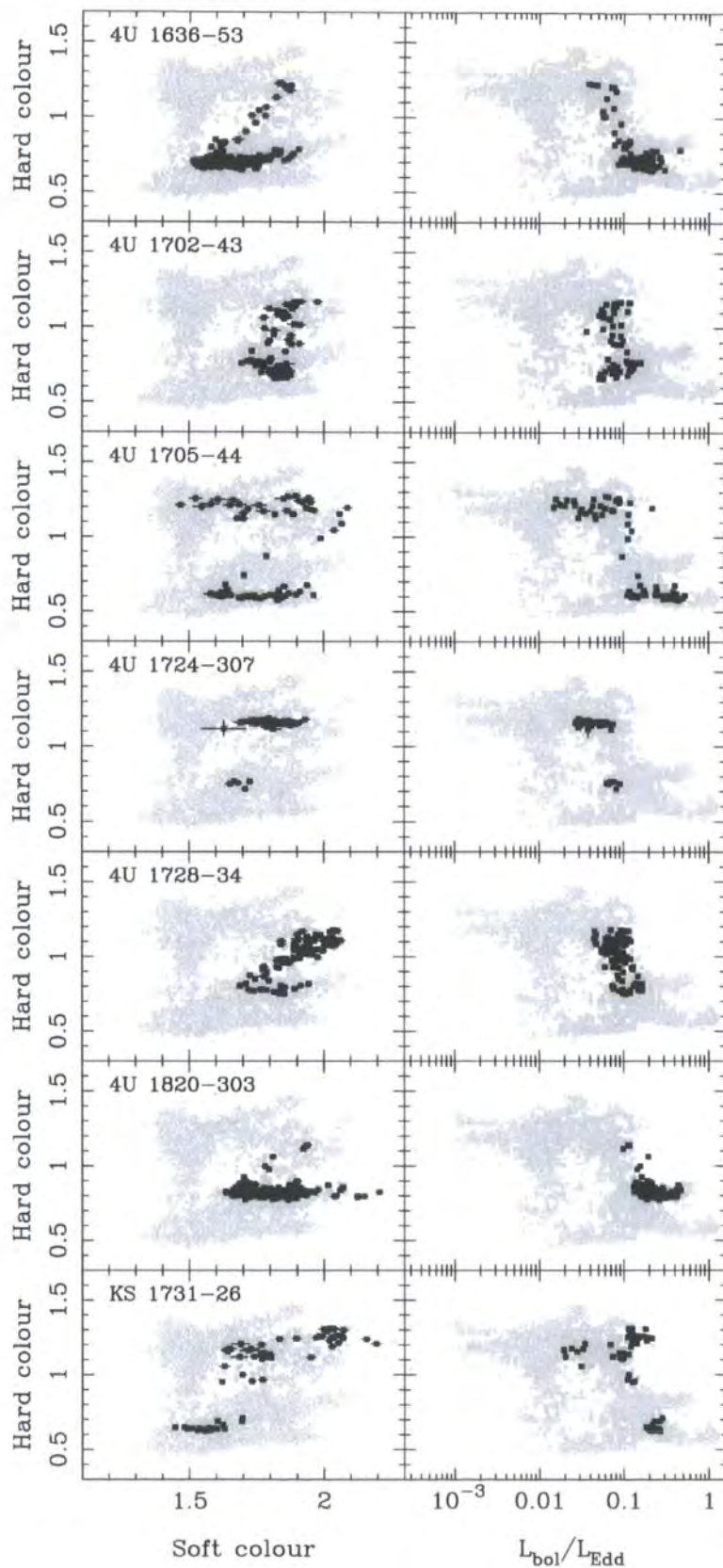Figure 7.4: Combined colour-colour colour-luminosity plots for the *RXTE* PCA data of all atoll sources with $N_H < 3 \times 10^{22} \mathrm{cm}^{-2}$ which display a diagonal transition from hard to soft state in the colour-colour diagram, plotted against a backdrop of all data.
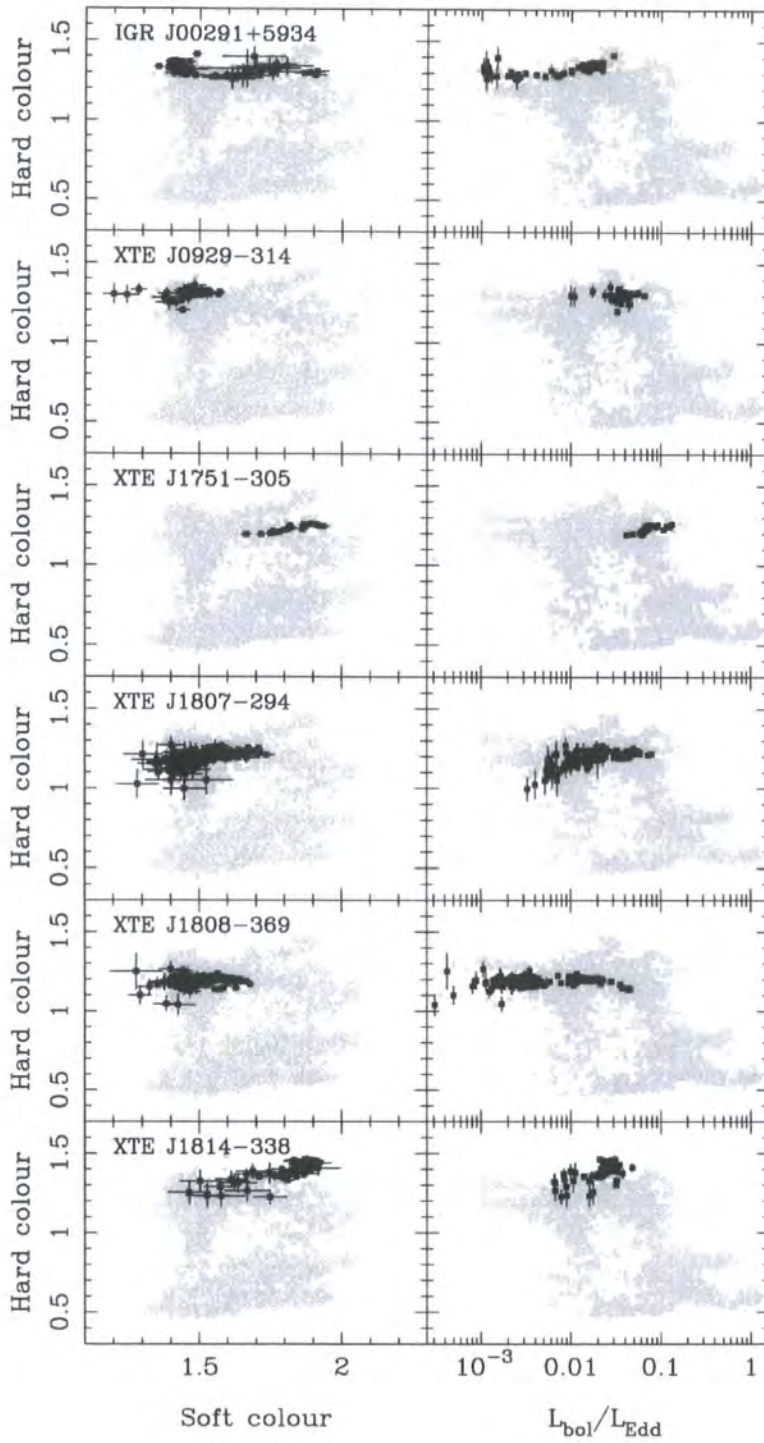
Figure 7.5: Combined colour-colour colour-luminosity plots for the *RXTE* PCA data of millisecond pulsars, plotted against a backdrop of all data.

We show this difference in transition behaviour by plotting the colour-colour and colour-luminosity diagrams for each individual source which shows a clear state transition. Those making a vertical transition are shown in figure 7.3, while those making a diagonal transition are shown in figure 7.4. Not all objects have data covering a transition. Some, such as all the millisecond pulsars, are only seen in the hard (island) state (see figure 7.5), others e.g. 4U 1735–44 are seen only in the soft (banana) branch. Of the ones which do make transitions, showing both hard and soft spectra, the effects of data windowing mean that not all have observations covering the transition period. Nonetheless, the size of the *RXTE* database mean there are 11 sources which do have enough data to constrain the shape of the transition on the colour-colour diagrams. The remaining sources, where there is insufficient transition data available at present are included in the background points plotted on each image and plotted individually in A.2 .

Chapter 8

Discussion

There are subtle differences in the spectral evolution of the atolls on the colour-colour and colour-luminosity diagrams. Firstly, there is the distinction between the transition track (verticals and diagonals). Secondly, within the diagonals there is a difference in spectral hardness of the banana branch, and within the verticals there are objects which show large scale hysteresis. Here we examine possible explanations for these effects.

8.1 Inclination

A range of inclinations is expected for these sources, and this could be important for the observed spectrum if the intrinsic emission is not isotropic. Some degree of anisotropy is certainly expected from the accretion disc due to its planar geometry, and as long as the boundary layer has a different angular dependence then the overall spectrum will change as a function of inclination.

To estimate the effects of inclination we use the spectral model consisting of the disc emission (DISKBB) and the optically thin boundary layer emission, which we model by thermal Comptonisation (COMPTT). Done & Gierliński in 2003, previously referred to as DG03, showed that the banana branch could be roughly characterized by a disc varying in temperature in the range 1.0–1.5 keV together with an equal luminosity boundary layer with $kT_e = 3$ keV and $\tau = 5$. We use these parameters to model the shape of the banana branch.

We first assume that the boundary layer is isotropic, while the disc normalization varies as $\cos i$ but with angle averaged luminosity equal to that of the boundary layer. Thus the apparent ratio of disc to boundary layer flux will change as the inclination
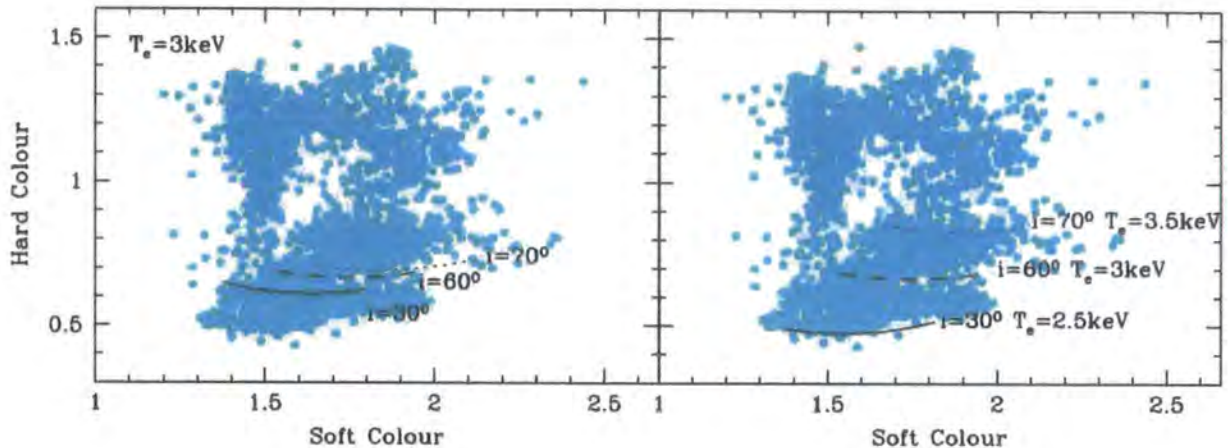
Figure 8.1: Colour-colour diagrams showing the effect of inclination on the position of the banana branch. The inclination is 30° (solid curves), 60° (dashed curves) and 70° (dotted curves). Each curve represents the disc plus boundary layer model, for the range of disc temperatures of 1.0–1.5 keV (see text for details). In panel (a) the disc emission is assumed to be angle-dependent, while the boundary layer emission is isotropic, with constant temperature of 3 keV. In panel (b) the boundary layer emission is assumed to be anisotropic, with higher observed temperature closer to the equator. The three curves correspond to the same inclination angles as in panel (a), but this time the boundary layer temperature is 2.5, 3.0 and 3.5 keV, for increasing angles, respectively.

angle varies. In figure 8.1(a) we show how the banana branch moves on the colour-colour diagram for inclinations of 30°, 60° and 70°. The change is mainly only in the soft colour, with a greater proportion of disc emission shifting the start of the banana branch to lower soft colours. Plainly this cannot account for either of the two subtle spectral effects seen, but seems to have more potential to explain the different positions of the banana branch amongst the diagonals rather than the difference between verticals and diagonals.

Examination of some of the individual banana branch spectra of the diagonals showed that the Comptonisation temperature of the boundary layer is also changing, and in a way

which is correlated with L_{disc}/L_{BL}. This could indicate that the boundary layer emission is itself anisotropic, perhaps with a temperature gradient so that it is hotter close to the equatorial plane where the disc hits the neutron star. Figure 8.1(b) shows the effect of changing the temperature of the boundary layer from 2.5, 3.0 and 3.5 keV, for inclination angles of 30°, 60° and 70°, respectively. This matches very well with the range of banana branches seen in the diagonals.

Testing this would require knowledge of the inclination, but very few sources have good enough orbital determinations to constrain this. However, any source exhibiting dips must be at fairly high inclination ($i > 70°$), and hence would be expected to have a banana branch starting at fairly large hard and soft colours. This can be seen in the case of 4U 1724-307 (see fig 7.4), a dipping source whose banana branch ranges from 1.65-1.75 in soft colour and 0.7 to 0.8 in hard colour. There are three other dipping sources, 4U 1704-30, 4U 1746-37 and 4U 1915-05, that also support this idea, with each exhibiting high and soft colours in the banana state (for CCD see A.2).

8.2 Spin

Burst oscillations and kHz QPOs have finally given observational constraints on LMXB neutron star spins (e.g. the review by van der Klis 2000). For our sample, the inferred range is from 330 to 619 Hz. However, this is unlikely to be the origin of the difference in transition track as the spins seem fairly evenly distributed between the two classes. Nonetheless, spin could give a difference in the overall luminosity/temperature of the boundary layer. Lower spin gives a higher relative speed between the inner edge of the disc and the surface, leading to a lower L_{disc}/L_{BL} ratio and a higher boundary layer temperature, as required for the different banana branch hard colours seen. Thus it seems likely that some combination of spin and inclination effects are responsible for the different banana branches seen in the diagonals, but neither is likely to explain the origin of the two different types of transition behaviour.

8.3 Transient Behaviour and Hysteresis

The ASM and PCA light curves show large scale transient outbursts only in 4U 1608–52, XTE J1806–246, 4U 1908+005 and all the millisecond pulsars. This is very intriguing as 4U 1608–52 and 4U 1908+005 are both verticals (there is insufficient data from XTE J1806–246 to determine whether its transition is vertical or diagonal). However, examination of the ASM lightcurves of the other verticals clearly shows that these objects do not undergo dramatic outbursts, so this cannot be the origin of the vertical/diagonal distinction.

However, 4U 1608–52 and 4U 1908+005 are also the only objects to show clear large-scale hysteresis (again, there is insufficient data from XTE J1806–246 whether or not it shows hysteresis). Thus it seems possible that hysteresis is linked to large amplitude outbursts. There are no counterexamples i.e. no systems which show disc outbursts which push the accretion rate high enough to make a spectral transition which do not show hysteresis. All the millisecond pulsar outbursts remain in the hard state, and no other atolls show outbursts with enough data to examine the transition for hysteresis.

This hypothesis can be tested on the black hole systems. Unlike the atolls, most of these are transients. This distinction in disc instability behaviour between black holes and neutron stars can be broadly explained in the context of the hydrogen ionisation models. Neutron stars are lower mass than black holes, so for the same companion star to overflow its Roche lobe requires a smaller binary orbit for a neutron star compared to a black hole. Smaller orbital separation means a smaller disc due to tidal truncation. The size of the disc, together with the mass loss rate from the companion star (determined by its evolutionary state) determines the temperature of the coolest part of the disc. Thus the smaller neutron star systems are less likely to have a disc which can drop below the hydrogen ionization temperature required to trigger the disc instability (King & Ritter 1998; King, Kolb & Szuszkiewicz 1997).

It is well known that most black hole systems show large scale hysteresis (e.g. Mac-

carone & Coppi 2003). Thus they support the idea above that hysteresis is linked to large amplitude outbursts. Even more support comes from the one obvious exception, which is Cyg X-1. This does not show hysteresis during its hard/soft transitions, and is of course a persistent source (e.g. Maccarone & Coppi 2003, DG03).

Maccarone & Coppi (2003) also suggested that hysteresis could be linked to large scale outbursts, but with only Cyg X-1 as an counterexample the connection to outbursts is not quite so unambiguous. Cyg X-1 is also one of the few known galactic black holes with a high mass companion, so there is the possibility that the accretion structure is somewhat different due to lower angular momentum material from a stellar wind. By contrast, with the neutron stars being generally stable to the hydrogen ionisation trigger for the disc outbursts, there are many counterexamples, all with low mass companions. We can rule out the alternative origin for hysteresis discussed by Maccarone & Coppi (2003), namely that it is produced simply by a difference in behaviour in low mass X-ray binaries between a hard–to–soft transition on the rising part of the light curve, and a soft–to–hard transition as the flux decreases. Most of the sources shown in figures 7.4 and 7.3 make the transition in both directions, and do not show large scale hysteresis (though there are smaller scale effects, consistent with the difference in environment: Meyer & Meyer-Hoffmeister 2005). Instead, hysteresis is seen where the mass accretion rate changes dramatically (from $\sim L/L_{\mathrm{Edd}} \ll 10^{-4}$ to 0.1). We speculate that the accretion flow is able to access non-equilibrium states during the rapid changes in accretion disc structure caused by the disc instability.

Thus the neutron stars clearly show a one–to–one correlation between the dramatic large amplitude outbursts triggered by the disc instability and hysteresis, consistent with this being the origin of hysteresis. This predicts that the millisecond pulsar outbursts should also show hysteresis if their accretion rate at the outburst peak ever goes high enough to trigger a spectral transition (in which case we would expect them also be verticals, along with 4U 1608–52 and 4U 1908+005). However, there is no such one–

to–one correlation between outbursts and transition behaviour (vertical/diagonal), so we explore further aspects of the systems below.

8.4 Binary System Parameters

Table 6.2 shows the binary parameters where these are known. We first explore whether there is any correlation between transition behaviour and binary period (which is a tracer of companion type, and also of superburst behaviour: Kuulkers et all 2004). For the verticals, the periods span a large range, from 1 hour for the persistent sources 4U 0614+091 and 4U 0919–54 through to 19 and 288 hours for the transients 4U 1608-52 and 4U 1908+005. This distinction is as expected from the disc instability model (wide binary implies a much larger disc, so a cooler outer edge which is more likely to trigger the hydrogen instability). If the millisecond pulsars are also verticals then these fill in the period distribution from 40 minutes to 4 hours. There is very little data to compare this to the diagonals, as only 2 have periods (11 minutes and 3.9 hours), but the broad span seen from the verticals encompasses most of the binary periods seen in atolls, so binary period alone (or companion type or the CNO enriched chemical composition of superbursts) is unlikely to be the origin of the transition track dichotomy.

8.5 Long Term Mass Accretion Rate

The distinction between millisecond pulsars, which plainly retain a residual magnetic field channelling the flow, and other atolls which do not show pulsations is most probably due to the long timescale mass accretion rate (Cumming, Zweibel & Bildsten 2001). Plausibly, high accretion rates can bury the magnetic field below the neutron star surface, but the very low average mass accretion rate in the millisecond pulsars is insufficient to bury the field (Cumming et al. 2001). Thus there is a potential physical mechanism for the long term mass accretion rate to change the properties of the accretion flow.

We estimate the long term mass accretion rate for all of the systems from the observed X-ray emission. The PCA data gives estimates for L_{bol} through spectral fitting, but the light curves are highly incomplete, so this data cannot simply be used as an indicator of the long term average mass accretion rate. By contrast, the *RXTE* All Sky Monitor (ASM) gives an almost continuous light curve for every bright X-ray source in its field of view, but its lack of spectral resolution means that going from count rate to L_{bol} is highly uncertain. Hence we combine the two approaches. We use the PCA light curve to define the average L_{bol}/L_{Edd} during these observations, then select the simultaneous ASM points to find the average ASM count rate during the PCA observations. The ratio of this to the full ASM light curve gives the correction for the incompleteness of the PCA observations.

This approach works well unless the source becomes very faint, in which case contamination of the ASM by other nearby sources and/or galactic ridge emission can be a problem. The only sources for which this is an issue are the transients i.e. the verticals 4U 1608-52 and 4U 1908+005 and all the millisecond pulsars. The outbursts of 4U 1608-52 and 4U 1908+005 are so bright that they dominate the average of the ASM lightcurves. However, this is not the case for the millisecond pulsars, so for these we use a different approach. Here we use the PCA data alone, assuming that the source intensity is negligible in the periods outside the known outbursts. The results of both the millisecond pulsars and atoll sources are shown in Table 8.1.

It can be seen that there is a systematic difference between the three classes of sources. The millisecond pulsars have the lowest long term average luminosity then the verticals, then the diagonals. Thus it seems possible that this is the origin of the difference in transition properties. The millisecond pulsars low long term mass accretion rate allows the field to diffuse out of the crust, and to be strong enough to collimate the flow and produce pulsations. One possibility might be that while the high average mass accretion rate of the diagonals suppresses the field entirely, the average mass accretion rate in the

Source Name	Source Type	$L_{\text{bol}}/L_{\text{Edd}}$
IGR J00291+5934	msp	1.4×10^{-5}
XTE J0929–314	msp	1.4×10^{-4}
XTE J1751–305	msp	5.2×10^{-5}
XTE J1807–294	msp	2.7×10^{-4}
XTE J1808–369	msp	6.7×10^{-5}
XTE J1814–338	msp	1.6×10^{-4}
4U 0614+091	V	3.2×10^{-3}
4U 0919–54	V	3.1×10^{-3}
4U 1608–52	V	6.6×10^{-3}
4U 1908+005	V	3.7×10^{-3}
SLX 1735–269	V	1.6×10^{-3}
4U 1636–53	D	4.4×10^{-2}
4U 1702–43	D	7.8×10^{-3}
4U 1705–44	D	1.9×10^{-2}
4U 1724–307	D	7.3×10^{-3}
4U 1728–34	D	1.9×10^{-2}
4U 1820–303	D	1.3×10^{-1}
KS 1731–26	D	3.4×10^{-2}

Table 8.1: Results of long term mass accretion rate calculations revealing a distinct break between millisecond pulsars (msp) and atoll sources as well as a more subtle break between sources where the hard–soft transition is approximately vertical on a colour-colour diagram (V) and those where it makes a diagonal track (D).

verticals allows some field to diffuse out. The problem with this is that the magnetic field cannot collimate any significant part of the flow in the verticals as these show no trace of pulsations.

One way around these pulsation limits is to separate the field and accretion flow. Any non-spherical accretion flow will predominantly bury the field in the region of the flow, leaving the field to escape in regions with little accretion. Even the hot accretion flow envisaged for the hard island states favours the equatorial plane, with a geometry which is more like a thick disc than a truly spherical flow (e.g. Narayan & Yi 1995). This nicely circumvents the pulsation limits, but then there is no interaction between the magnetic field and the flow, and so no physical mechanism to change the behaviour of the transition.

However, one aspect of the system that a polar magnetic field could affect is the jet. The most recent numerical simulations of the accretion flow magnetohydrodynamics show a causal link between the jet and accretion flow (Hawley & Krolik 2006; McKinney 2006), so this might give an indirect link between the magnetic field and accretion flow properties. One way to test this is to look at the radio emission from these systems. While theoretical models of jets are not well developed, we can use the observed galactic black hole behaviour as a template. These show a clear correlation between radio and X-ray luminosity in their low/hard state, showing that L_x/L_{Edd} is important in determining the power of the jet (Gallo, Fender and Pooley 2003). Hence to see whether there are differences in the jet emission between the millisecond pulsars, verticals and diagonals we need to compare the radio emission at the same L_x/L_{Edd}. Hysteresis gives potential problems (Maccarone & Coppi 2003), so ideally the comparison would be between persistent verticals and diagonals in the hard island state at the same L_x. However, there is very little data to make this comparison, with only 4U 0614+091 and 4U 1728-34 for the persistent verticals and diagonals, respectively, and these do not overlap in L_x (Migliari & Fender 2006). Thus we speculate that the origin of the difference in transition behaviour between the verticals and diagonals is due to the presence of some magnetic field at the pole in the verticals which

affects the accretion flow indirectly through jet formation, by contrast to the diagonals which have higher mass accretion rates, sufficient to bury the field everywhere.

Chapter 9 | *Conclusions*

The atolls and millisecond pulsars are consistent with showing the same overall spectral evolution with changing mass accretion rate, but there are some slight but significant differences. The spectral shape of the soft (banana) branch shows subtle variations from object to object, most probably due to combination of inclination and spin changing the ratio of the observed disc to boundary layer luminosity, and boundary layer temperature. However, there are also clear differences in behaviour during the hard/soft transition which point to a more fundamental distinction. The data shows two types of sources, those where the transition follows a vertical track on the colour-colour diagram, and occurs at $L/L_{\rm Edd} \sim 0.02$, and those which make a diagonal track on the colour-colour diagram with the transition at $L/L_{\rm Edd} \sim 0.1$. There are hysteresis effects in individual sources which introduce dispersion in the transition luminosity, but these are large *only* for the outbursting atolls (which are both verticals). Splitting these outbursts into the rapid rise and slow decay phases show that the rapid rise looks like the millisecond pulsars (so they are probably also verticals) while the slow decay looks like the persistent verticals. Thus it seems likely that large scale hysteresis effects are only seen in sources where the disc structure changes rapidly due to the onset of the hydrogen ionization instability. This is also consistent with the observed black hole behaviour. The association of the millisecond pulsars with verticals suggests that the difference in transition is ultimately linked to the surface magnetic field, and indeed, all the verticals have long term mass accretion rates which are smaller than those of the diagonals, though not as small as those of the millisecond pulsars. Thus the verticals could have some small magnetic field which is able to affect the inner accretion flow, but this must be indirect as otherwise these systems also would show pulsations. We speculate that the physical link between

57

the magnetic field (predominantly polar) and accretion flow (predominantly equatorial) may be due to the changes in the jet, which would be testable with more radio data on these sources.

Chapter 10 | *Looking to the Future*

As this section of research draws to an end it opens new doorways to possible future research. This work looked in detail at low magnetic field disc accreting neutron stars (namely atoll sources). The conclusions drawn from this are that the increase in long term mass accretion rate from millisecond pulsars to verticals and then diagonals may suppress surface magnetic fields causing changes in the jet and the accretion flow. This would require radio surveys of sources in each category, i.e. msp, verticals and diagonals, to test.

This is just one suggestion for the future development of this work. Another option would be to extend the survey to include Z sources, with the initial aim being to gain an overview of their behaviour (as has been done here with the atolls). Once this was complete attention could be turned to those low magnetic field, disc accreting neutron star objects not yet (completely) classified. These are objects that display aspects of both types of object such as Cir X-1 which has been described as a Z type source until recently when the mass accretion rate dropped changing the properties observed, there is also the Z source discovered recently (XTE J1701-462) that is a transient. Are these sources Zs at low L/L_{Edd}? Are they atolls? Are they something else, a third type of low mass x-ray binary or do they bridge the gap between these two types of sources, unifying neutron stars in low mass binary systems into only one category varying only in mass accretion rate.

Chapter A

Appendix

A.1 Sources not included in sample selection

Table A.1 that shows those low magnetic, disc accreting neutron star sources not included in the sample selection and the reasons for their exclusion. Objects that were affected by heavy absorption ($N_H > 3 \times 10^{22}$ cm^{-2}) were ignored as their spectral decomposition would be uncertain, this discounts those too heavily absorbed by material in the galactic plane, accretion disc coronal sources and those affected by excessive dipping (to a degree where most observations would be affected by dips) although those sources which displayed limited dipping were included with the contaminated spectra removed. One recently discovered millisecond pulsar appears in table A.1 as there are currently no observations listed public RXTE archive for this source and hence it is excluded from the sample selection. Finally Z-sources were removed as we are only interested in the range $10^{-3} < L/L_{Edd} < 1$ to compare with the galactic black hole sources.

Source Name	N_H $(10^{22}$ cm$^{-2})$	Distance (kpc)	Reason for not Including	Dips	Period (hrs)	Spin (Hz)	References
2S 0921–630	0.17	7	ADC	Y	9		1,2,4,5
4U 1624–49	8.6	15	ADC/N_H	Y	0.35		1,3,6,7,8
4U 1822–371	0.05	2–3	ADC	Y			1,9
EXO 0748–676	0.8	5.9	Dips	Y	3.82	45	3,10,11,12,13,14
GRO J1744–28	5–6	8	N_H				1,15,16
GRS 1747–312	4–5	9.5	N_H	Y	12.4		17,18,19
MS 1603+206	1.5	6	ADC	Y			20
SAX J1747.0-2853	9.81	9	N_H				21
HETE J1900.1-2455	0.15	5	NA		1.38	377	22,23
Cir X-1			Z-source				24
Cyg X-2			Z-source				24
GX 5-1			Z-source				24
GX 17+2			Z-source				24
GX 340+0			Z-source				24
GX 349+2			Z-source				24
LMC X-2			Z-source				24
Sco X-1			Z-source				24

Table A.1: A list of atoll (first section) and millisecond pulsar (middle section) and Z (bottom section) sources that are not included in the analysis of data for this paper and reasons for non inclusion. ADC = accretion disc coronal source, Dips = Persistent dipper showing contamination in most observations, N_H = Column density is too high so that source is heavily absorbed, NA = archival data not yet publicly available and Z-source = displays properties and characteristics of a Z source. References: [1]Liu et al. 2001, [2]Christian & Swank 1997, [2]Diaz Trigo et al. 2005, [4]Jonker et al. 2004, [5]Kallman et al. 2002, [6]Parmar et al. 2002, [7]Smale at al 2000, [8]Owens et al. 1997, [9]Parmar et al. 2000, [10]Homan et al. 2003, [11]Wolff et al. 2002, [12]Wolff et al. 2005, [13]Villarreal & Strohmayer 2004, [14]Garcia et al. 2001, [15]Nishiuchi et al. 2000, [16]Manchanda & Rao 2001, [17]Galloway at al. 2003, [18]t Zand et al 2000, [19]t Zand et al. 2003, [20]Jonker et al. 2003, [21]Natalucci et al 2004. [22]Poutanen 2005, [23]Kaaret et al 2006, [24]Hassinger & van der Klis 1989.

A.2   Colour-Colour and Colour-Luminosity Plots

The following pages contain the colour-colour and colour-luminosity plots not displayed individually in the main body of the text, although their data is included in the background of all plots. The reason for there exclusion from the main body of the text is that current observations show that they either reside only in one state or that data windowing has meant that we have not yet observed which transitional track they follow. Each plot is shown against a background of all processed data.
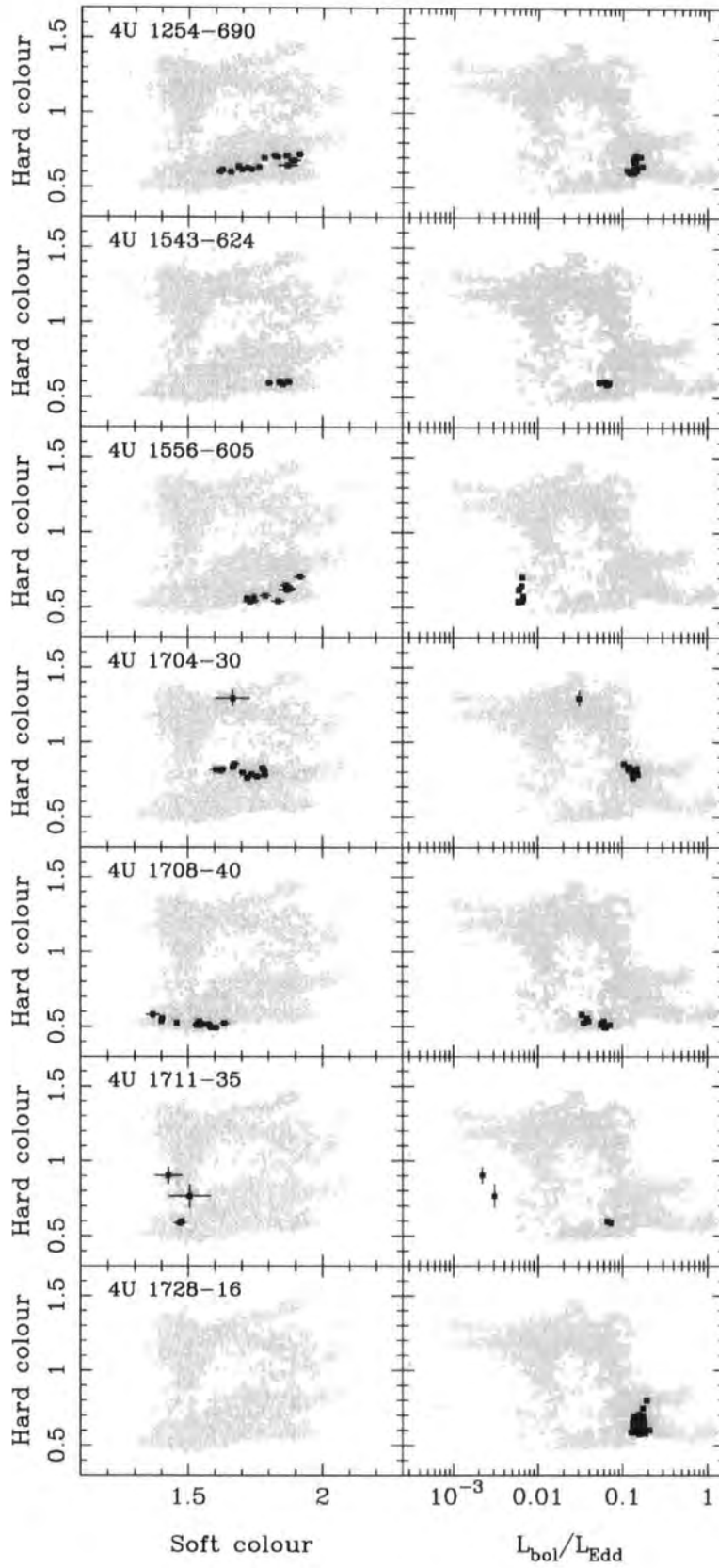
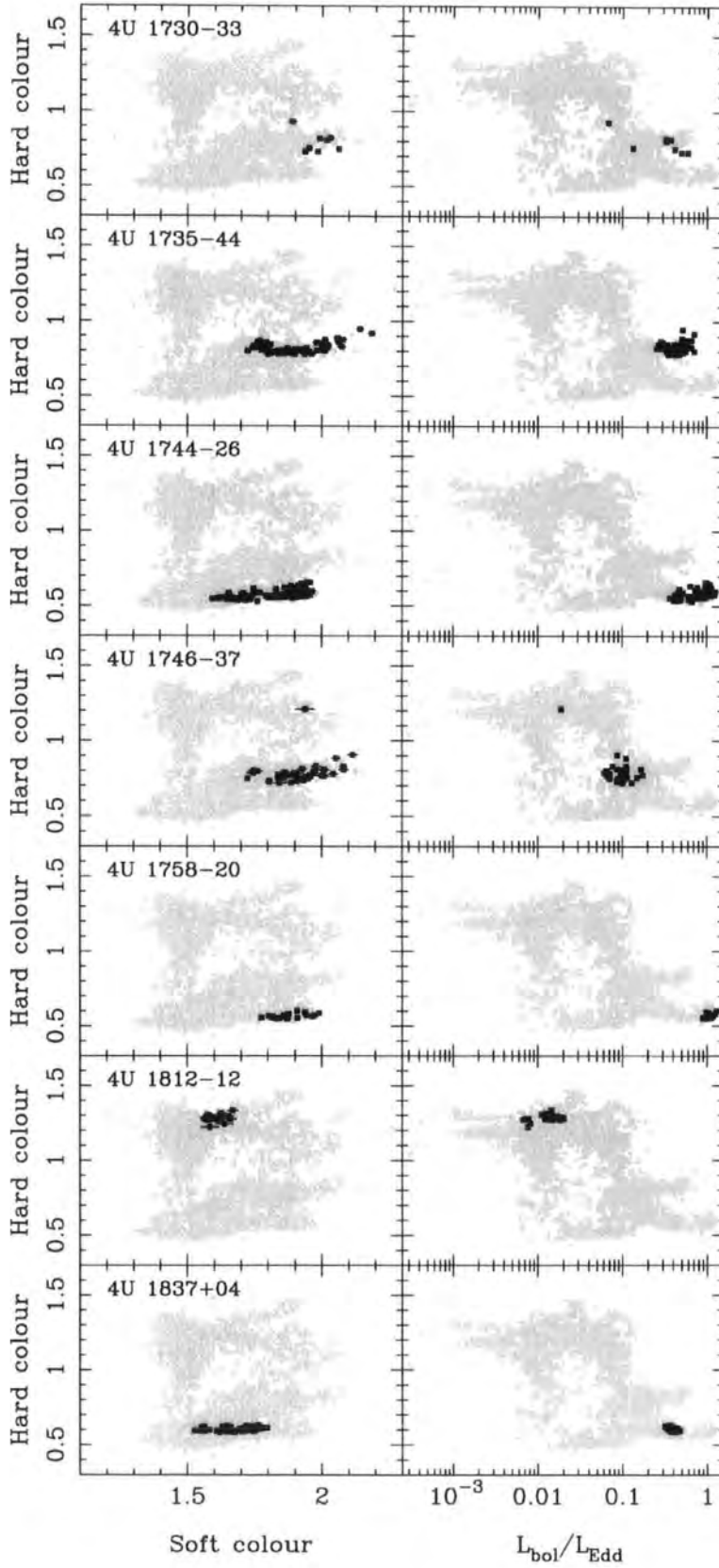Figure A.1: CC/CL plots for all sources not previously included.

Figure A.2: CC/CL plots for all sources not previously included.
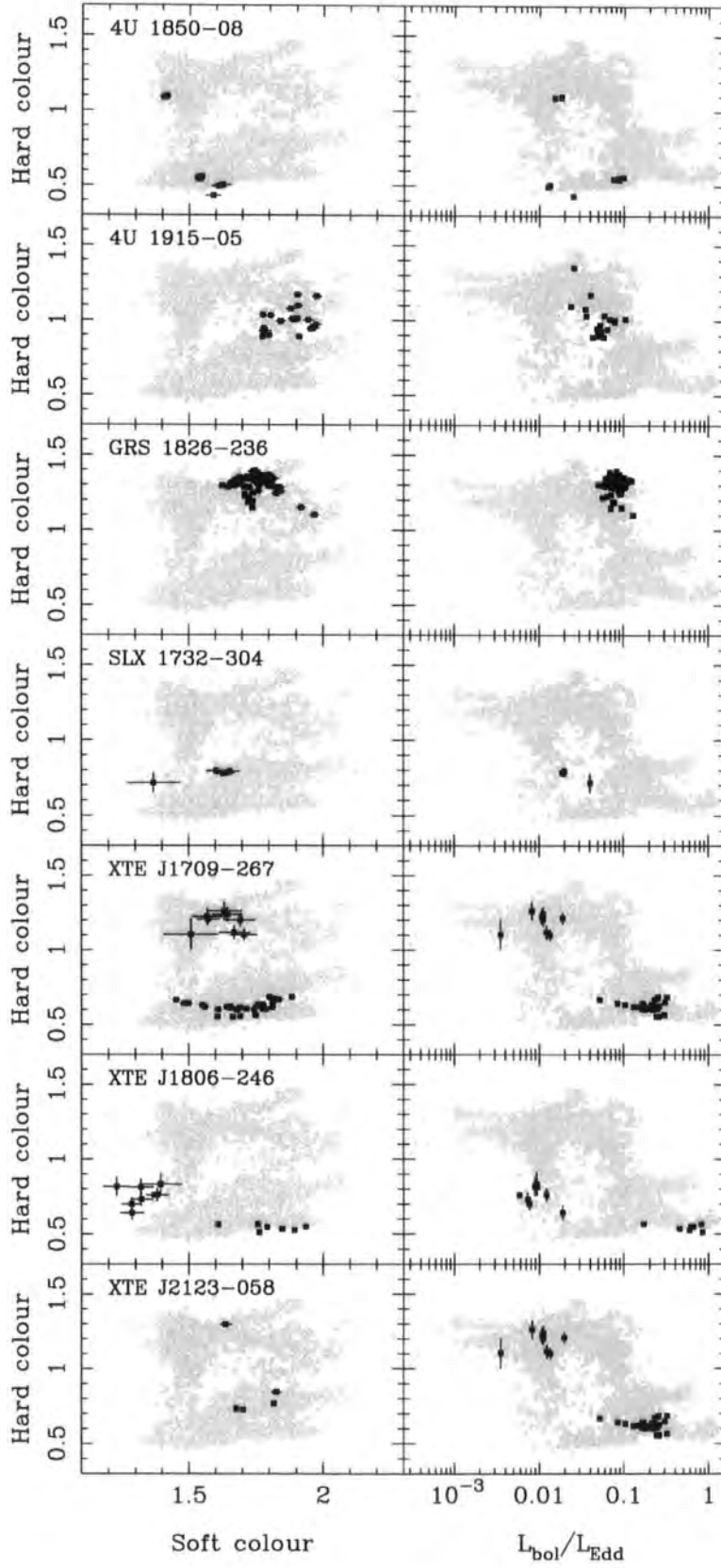
Figure A.3: CC/CL plots for all sources not previously included.

Bibliography

[1] Angelini L., White N. E., Nagase F., Kallman T. R., Yoshida A., Takeshima T., Becker C., Paerels F., 1995, ApJ, 449, L41

[2] Bałucińska-Church, M., Church, M. J., & Smale, A. P. 2004, MNRAS, 347, 334

[3] Barret, D., & Vedrenne, G. 1994, ApJS, 92, 505

[4] Barret, D., Olive, J. F., Boirin, L., Done, C., Skinner, G. K., & Grindlay, J. E. 2000, ApJ, 533, 329

[5] Barret, D., Olive, J. F., & Oosterbroek, T. 2003, A&A, 400, 643

[6] Bloser, P. F., Grindlay, J. E., Barret, D., & Boirin, L. 2000, ApJ, 542, 989

[7] Burderi, L., et al. 2002, ApJ, 574, 930

[8] Campana, S., Ferrari, N., Stella, L., & Israel, G. L. 2005, A&A, 434, L9

[9] Chevalier, C., Ilovaisky, S. A., Leisy, P., & Patat, F. 1999, A&A, 347, L51

[10] Christian, D. J., & Swank, J. H. 1997, ApJS, 109, 177

[11] Courvoisier, T. J.-L., Parmar, A. N., Peacock, A., & Pakull, M. 1986, ApJ, 309, 265

[12] Cumming, A., Zweibel, E., & Bildsten, L. 2001, ApJ, 557, 958

[13] Di Salvo, T., Iaria, R., Burderi, L., & Robba, N. R. 2000, ApJ, 542, 1034

[14] Di Salvo, T., Iaria, R., Méndez, M., Burderi, L., Lavagetto, G., Robba, N. R., Stella, L., & van der Klis, M. 2005, ApJ, 623, L121

[15] Díaz Trigo, M., Parmar, A. N., Boirin, L., Méndez, M., & Kaastra, J. S. 2006, A&A, 445, 179

[16] Done, C., & Gierliński, M. 2003, MNRAS, 342, 1041

[17] Emelyanov, A. N., Revnivtsev, M. G., Aref'ev, V. A., & Sunyaev, R. A. 2002, Astronomy Letters, 28, 12

[18] Falanga, M., Farinelli, R., Goldoni, P., Frontera, F., Goldwurm, A., & Stella, L. 2004, A&A, 426, 979

[19] Falcke, H., Körding, E., & Markoff, S. 2004, A&A, 414, 895

[20] Farinelli, R., et al. 2003, A&A, 402, 1021

[21] Fender, R. P., & Hendry, M. A. 2000, MNRAS, 317, 1

[22] Gallo, E., Fender, R. P., & Pooley, G. G. 2003, MNRAS, 344, 60

[23] Galloway, D. K., Chakrabarty, D., Muno, M. P., & Savov, P. 2001, ApJ, 549, L85

[24] Galloway, D. K., Cumming, A., Kuulkers, E., Bildsten, L., Chakrabarty, D., & Rothschild, R. E. 2004, ApJ, 601, 466

[25] Garcia, M. R., McClintock, J. E., Narayan, R., Callanan, P., Barret, D., & Murray, S. S. 2001, ApJ, 553, L47

[26] Gierliński, M., & Done, C. 2002, MNRAS, 331, L47

[27] Gierliński, M., & Poutanen, J. 2005, MNRAS, 359, 1261

[28] Hasinger, G., & van der Klis, M. 1989, A&A, 225, 79

[29] Homan, J., Wijnands, R., & van den Berg, M. 2003, A&A, 412, 799

[30] Homer L., Charles P. A., Naylor T., van Paradijs J., Auriere M., Koch-Miramond L., 1996, MNRAS, 282, L37

[31] in't Zand, J. J. M., Strohmayer, T. E., Markwardt, C. B., & Swank, J. 2003, A&A, 409, 659

[32] in't Zand, J. J. M., Kuulkers, E., Verbunt, F., Heise, J., & Cornelisse, R. 2003, A&A, 411, L487

[33] Jonker, P. G., van der Klis, M., Homan, J., Wijnands, R., van Paradijs, J., Méndez, M., Kuulkers, E., & Ford, E. C. 2000, ApJ, 531, 453

[34] Jonker, P. G., et al. 2001, ApJ, 553, 335

[35] Jonker, P. G., van der Klis, M., Kouveliotou, C., Méndez, M., Lewin, W. H. G., & Belloni, T. 2003, MNRAS, 346, 684

[36] Jonker, P. G., Galloway, D. K., McClintock, J. E., Buxton, M., Garcia, M., & Murray, S. 2004, MNRAS, 354, 666

[37] Jonker, P. G., Steeghs, D., Nelemans, G., & van der Klis, M. 2005, MNRAS, 356, 621

[38] Jonker, P. G., Campana, S., Steeghs, D., Torres, M. A. P., Galloway, D. K., Markwardt, C. B., Chakrabarty, D., & Swank, J. 2005, MNRAS, 361, 511

[39] Juett, A. M., & Chakrabarty, D. 2003, ApJ, 599, 498

[40] Kallman, T. R., Angelini, L., Boroson, B., & Cottam, J. 2003, ApJ, 583, 861

[41] King, A. R., Kolb, U., & Szuszkiewicz, E. 1997, ApJ, 488, 89

[42] King, A. R., & Ritter, H. 1998, MNRAS, 293, L42

[43] Krauss, M. I., et al. 2005, ApJ, 627, 910

[44] Krolik, J. H., Hawley, J. F., & Hirose, S. 2005, ApJ, 622, 1008

[45] Kuulkers, E., in't Zand, J., Homan, J., van Straaten, S., Altamirano, D., & van der Klis, M. 2004, AIP Conf. Proc. 714: X-ray Timing 2003: Rossi and Beyond, 714, 257

[46] Liu, Q. Z., van Paradijs, J., & van den Heuvel, E. P. J. 2001, A&A, 368, 1021

[47] Maccarone, T. J., & Coppi, P. S. 2003, MNRAS, 338, 189

[48] Maccarone, T. J., & Coppi, P. S. 2003, A&A, 399, 1151

[49] Manchanda, R. K., & Rao, A. R. 2001, Advances in Space Research, 28, 337

[50] McClintock, J. E., Narayan, R., & Rybicki, G. B. 2004, ApJ, 615, 402

[51] Mignani, R. P., Chaty, S., Mirabel, I. F., & Mereghetti, S. 2002, A&A, 389, L11

[52] Migliari, S., et al. 2003, MNRAS, 342, 909

[53] Migliari, S., van der Klis, M., & Fender, R. P. 2003, MNRAS, 345, L35

[54] Mitsuda, K., et al. 1984, PASJ, 36, 741

[55] Molkov, S. V., Grebenev, S. A., & Lutovinov, A. A. 2000, A&A, 357, L41

[56] Molkov, S., Revnivtsev, M., Lutovinov, A., & Sunyaev, R. 2005, A&A, 434, 1069

[57] Muno, M. P., Remillard, R. A., & Chakrabarty, D. 2002, ApJ, 568, L35

[58] Narayan, R., Yi, I., & Mahadevan, R. 1996, A&AS, 120, 287

[59] Narayan, R., & Heyl, J. S. 2002, ApJ, 574, L139

[60] Narayan, R. 2005, New Journal of Physics, 7, 199

[61] Nelemans, G., Jonker, P. G., Marsh, T. R., & van der Klis, M. 2004, MNRAS, 348, L7

[62] Nishiuchi, M., et al. 2000, Advances in Space Research, 25, 391

[63] Nowak, M. A. 1995, PASP, 107, 1207

[64] Oosterbroek, T., Parmar, A. N., Sidoli, L., in't Zand, J. J. M., & Heise, J. 2001, A&A, 376, 532

[65] Owens, A., Oosterbroek, T., & Parmar, A. N. 1997, A&A, 324, L9

[66] Park, S. Q., Miller, J. M., McClintock, J. E., & Murray, S. S. 2005, ApJ, 618, L45

[67] Parkinson, P. M. S., et al. 2003, ApJ, 595, 333

[68] Parmar, A. N., Oosterbroek, T., Del Sordo, S., Segreto, A., Santangelo, A., Dal Fiume, D., & Orlandini, M. 2000, A&A, 356, 175

[69] Parmar, A. N., Oosterbroek, T., Boirin, L., & Lumb, D. 2002, A&A, 386, 910

[70] Pavlinsky, M. N., Grebenev, S. A., Lutovinov, A. A., Sunyaev, R. A., & Finoguenov, A. V. 2001, Astronomy Letters, 27, 297

[71] Piro, A. L., & Bildsten, L. 2005, ApJ, 629, 438

[72] Revnivtsev, M., Borozdin, K., & Emelyanov, A. 1999, A&A, 344, L25

[73] Shaposhnikov, N., Titarchuk, L., & Haberl, F. 2003, ApJ, 593, L35

[74] Shaposhnikov, N., & Titarchuk, L. 2004, ApJ, 606, L57

[75] Sidoli, L., La Palombara, N., Oosterbroek, T., & Parmar, A. N. 2005, A&A, 443, 223

[76] Schultz, J. 2003, A&A, 397, 249

[77] Schulz, N. S. 1999, ApJ, 511, 304

[78] Smale, A. P., Church, M. J., & Bałucińska-Church, M. 2001, ApJ, 550, 962

[79] Smale, A. P., Church, M. J., & Bałucińska-Church, M. 2002, ApJ, 581, 1286

[80] Strohmayer, T. E., Markwardt, C. B., Swank, J. H., & in't Zand, J. 2003, ApJ, 596,
     L67

[81] Sunyaev, R., & Revnivtsev, M. 2000, A&A, 358, 617

[82] Tomsick, J. A., Gelino, D. M., Halpern, J. P., & Kaaret, P. 2004, ApJ, 610, 933

[83] van der Klis, M. 2000, ARA&A, 38, 717

[84] Wang, Z., & Chakrabarty, D. 2004, ApJ, 616, L139

[85] Wijnands, R., & van der Klis, M. 1999, A&A, 345, L35

[86] Wijnands, R., & van der Klis, M. 1999, ApJ, 522, 965

[87] Wijnands, R. 2001, ApJ, 554, L59

[88] Wijnands, R. 2003, ApJ, 588, 425

[89] Wijnands, R., Strohmayer, T., & Franco, L. M. 2001, ApJ, 549, L71

[90] Wolff, M. T., Hertz, P., Wood, K. S., Ray, P. S., & Bandyopadhyay, R. M. 2002,
     ApJ, 575, 384

[91] Wolff, M. T., Becker, P. A., Ray, P. S., & Wood, K. S. 2005, ApJ, 632, 1099

[92] Yao, Y., & Wang, Q. D. 2005, ApJ, 624, 751

[93] Zdziarski, A. A., Gierliński, M., Gondek, D., & Magdziarz, P. 1996, A&AS, 120, 553